2008-08-13

Tooth Engagement Evaluation of Involute Spline Couplings

Robert R. Robins
Brigham Young University - Provo

TOOTH ENGAGEMENT EVALUATION OF INVOLUTE SPLINE COUPLINGS

by

Robert Rich Robins

A thesis submitted to the faculty of

Brigham Young University

in partial fulfillment of the requirements for the degree of

Master of Science

Department of Mechanical Engineering

Brigham Young University

December 2008

BRIGHAM YOUNG UNIVERSITY

GRADUATE COMMITTEE APPROVAL

of a thesis submitted by

Robert Rich Robins

This thesis has been read by each member of the following graduate committee and by majority vote has been found to be satisfactory.

Date	Kenneth W. Chase, Chair
Date	Robert H. Todd
Date	Carl D. Sorensen

BRIGHAM YOUNG UNIVERSITY

As chair of the candidate's graduate committee, I have read the thesis of Robert Rich Robins in its final form and have found that (1) its format, citations, and bibliographical style are consistent and acceptable and fulfill university and department style requirements; (2) its illustrative materials including figures, tables, and charts are in place; and (3) the final manuscript is satisfactory to the graduate committee and is ready for submission to the university library.

Date

Kenneth W. Chase
Chair, Graduate Committee

Accepted for the Department

Larry L. Howell
Graduate Coordinator

Accepted for the College

Alan R. Parkinson
Dean, Ira A. Fulton College of
Engineering and Technology

ABSTRACT

TOOTH ENGAGEMENT EVALUATION OF

INVOLUTE SPLINE COUPLINGS

Robert Rich Robins

Department of Mechanical Engineering

Master of Science

Spline couplings are used in applications involving high torque; however, due to variations in teeth clearances, all teeth in spline couplings do not engage simultaneously, causing some of the teeth to carry a disproportionately large portion of the total load. Variations in tooth-to-tooth clearances mean the first pair of teeth to engage will carry more load and fail sooner. This has lead to an industry practice of designing splines around the criteria that only 25-50% of the teeth on a spline coupling will engage and carry the load, and the load is generally assumed to be uniformly distributed. This research on tooth engagement is part of an ongoing study sponsored by an industrial partner with the intent to more accurately describe and improve tooth engagement in spline couplings.

Tooth engagement in involute spline couplings is difficult to predict due to the complex geometry and even more complex manufacturing processes. Although manufacturing is closely controlled, with precision tooling, engagement problems persist. Presented herein is a detailed study of an involute spline coupling and its associated errors. Mating internal and external involute splines have been analyzed in order to identify variation and error patterns associated with spline coupling assemblies. These error patterns aid in understanding the manufacturing processes and ways in which we can better understand and predict tooth engagement.

Spline manufacturing processes were studied in an attempt to relate tooling and processing errors to the resultant error patterns observed in production couplings. Some correlation with tooth engagement measurements have been found, but significant differences remain unexplained. Tooth engagement measurements exhibited anomalous behavior, which raised questions about test apparatus and procedures.

The main contributions of this work are: A process for analytically creating torque-deflection curves in any configuration using measurement data, confirmation of the analytical tooth engagement sequence model from measured variation data, a better understanding of the experimental results, how to design future experimental tests, and the importance of early quasi-simultaneous tooth engagement.

Several valuable insights have resulted in a better understanding of the mechanics of tooth engagement and load-sharing among spline teeth. The progress made should encourage further study, which may lead to processes which are better understood and controlled, and to designs which are more robust to variation, with more predictable performance and improved load-carrying capacity.

ACKOWLEGDMENTS

It is with many thanks that I express gratitude to all who have participated and supported this research. I give special thanks to my wife and family for their inspiration and love, to my thesis advisor Dr. Ken Chase for his guidance and direction, and to the industrial sponsor of this research for their ongoing support. I would also like to offer my gratitude to my mother-in-law, whose service to my family and new-born baby has been invaluable. In addition, I give recognition to the help provided from Mike Tennutti, a gear process geometrician, and the members of my thesis committee, Dr. Todd and Dr. Sorensen. The list of individuals who have sustained and inspired me throughout this work goes on, and to them I also offer no less of my sincere appreciation.

TABLE OF CONTENTS

LIST OF TABLES

LIST OF FIGURES

Chapter 1 Introduction

Spline couplings, as shown in Figure 1-1, are used in applications involving high torques; however, due to variations in teeth clearances, all teeth in spline couplings do not engage simultaneously causing some of the teeth to carry a disproportionately large portion of the total load. These variations in tooth-to-tooth clearances mean the first pair of teeth to engage will carry more load and fail sooner. This has lead to an industry practice of designing splines around the criteria that 25-50% of the teeth on a spline coupling will engage and carry the load, and it is assumed to be uniformly distributed. This research on tooth engagement is part of an ongoing study sponsored by an industrial partner with the objective to accurately describe and improve tooth engagement in spline couplings in order to increase their load capacity and durability.

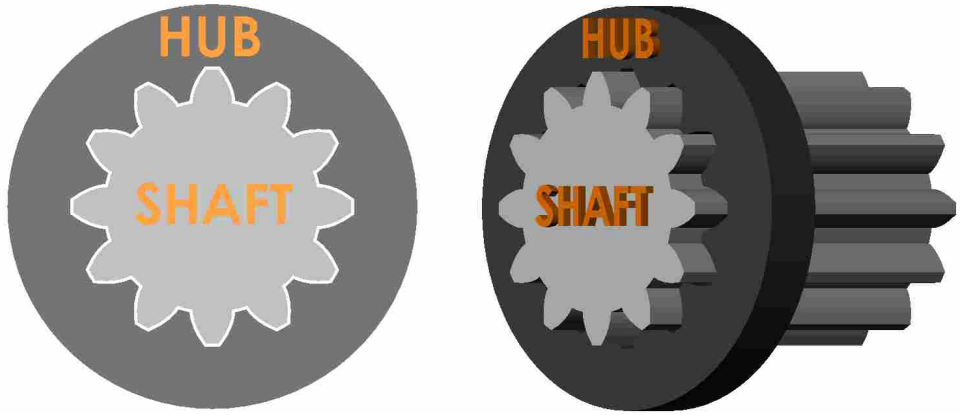

Figure 1-1 Example of a spline coupling

In spline couplings, torque is transferred from shaft to hub as the flanks of the mating teeth engage. Splines have precision teeth spaced uniformly around the full circumference of the shaft; therefore, the load capacity is greatly increased, compared to an ordinary keyway type coupling. In theory, all teeth engage at the same time and the load is carried equally between all tooth pairs.

With ideal tooth engagement there is a linear relationship between torque and angular deflection. As a torque is applied, all the teeth engage simultaneously and deflect proportional to the torque that is applied. The stiffness of four engaged teeth is four times the stiffness of a single tooth and each tooth carries 25% of the load, as shown in Figure 1-2.

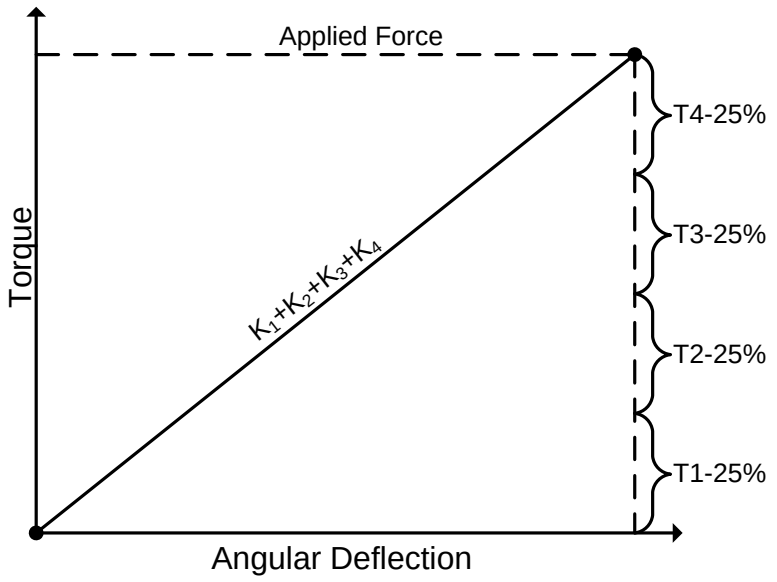

Figure 1-2 Theoretical tooth engagement profile of an ideal spline coupling

This ideal curve does not occur in practice due to tooth spacing variation, Figure 1-3 shows the effect of these variations. The four black lines represent four separate

tooth pairs. The slope of each line represents the equivalent stiffness of the tooth pair. The slopes (stiffness) of lines K_1, K_2, K_3, and K_4 are equal because tooth pairs are geometrically equivalent. However, while the tooth pairs maintain equivalent slopes, they start at different locations along the horizontal access. These differing starting points are the result of different tooth pair clearances that arise from manufacturing process variation. As a result of very small variations, the four tooth pairs do not engage simultaneously, rather the first tooth pair (T_1) engages and then begins to deflect until T_2 engages, T_1 and T_2 continue to deflect until T_3 engages, and so on. This process continues until all tooth pairs have engaged.

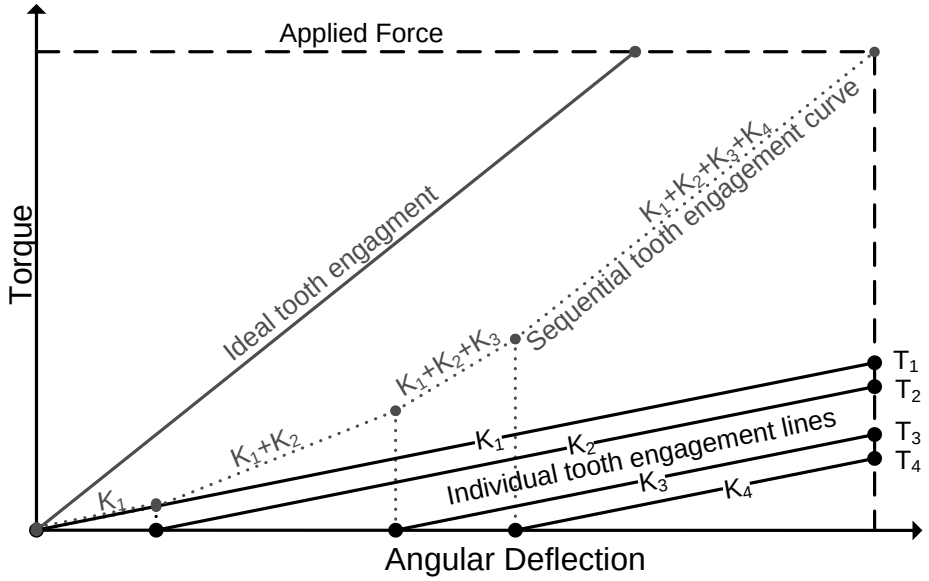

Figure 1-3 Sequential tooth engagement compared to ideal tooth engagement

The sequential tooth engagement curve, shown in Figure 1-3, is formed from the sum of the individual tooth engagement lines K_1-K_4 (note the differences between the ideal tooth engagement line and the sequential tooth engagement curve).

1.1 Background

Previous work in this investigation developed a sequential tooth engagement model (STEM), which allows designers to more accurately estimate tooth engagement and resulting stress based on a statistical representation of the tooth errors [7]. Process variations create errors in tooth index position, tooth profile, tooth-to-tooth spacing, and other geometric errors in both the shaft and the hub. The result is a variation in the clearances between each pair of mating teeth as shown in Figure 1-4. This variation in tooth pair clearances causes the teeth to engage sequentially, beginning with the pair having the least clearance and ending with the pair having the greatest clearance.

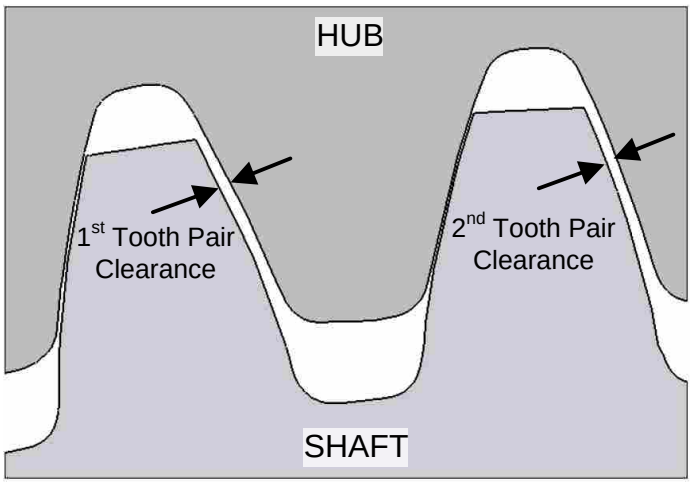

Figure 1-4 Variation in tooth pair clearance

Because of variation in tooth pair clearances, the load carried by each tooth pair will differ. Figure 1-5 shows a sequential tooth engagement profile and the resulting load carried by each of the four teeth. Tooth 1 carries 35% of the total load while tooth 4

carries only 15%. Due to variation, the first tooth to engage will carry significantly more load than the last tooth.

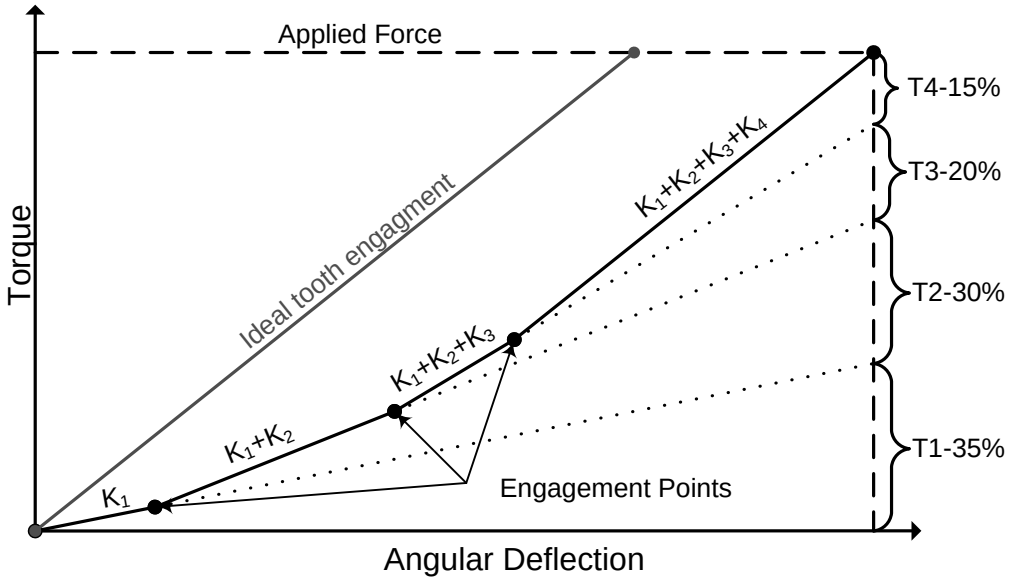

Figure 1-5 Percent load carried by each tooth in sequential tooth engagement

The amount of load carried by a given tooth pair can be found by extending the slope of each line segment, at the engagement points, then measuring the vertical distance between segments at the deflection value that results from the applied force.

Engagement points will differ for every spline assembly, because no two splines are identical. However, by modeling the variation in clearance statistically, the variation in the tooth engagement sequence can be predicted analytically and the bounds of variation established. Furthermore, if a single shaft and hub assembly is disassembled, and the shaft is incremented one tooth and reassembled, a new configuration is produced with a slightly different engagement sequence. So, a 10 tooth spline can produce 10 unique sequences for the same pair of components. And the same shaft, mated with 100

different hubs would have 1000 possible configurations, as would each of the other 99 shafts. All of these configurations may be modeled statistically by analyzing the variation in a single assembly, using the method developed at BYU [7].

1.2 Research Motivation

Figure 1-6 shows the experimental results of a test carried out by the industrial partner of this research. The test results display an interesting curve with increasing and decreasing slopes which raises the question of how the experiment was setup and suggests the possibility of error clustering wherein multiple teeth engage simultaneously.

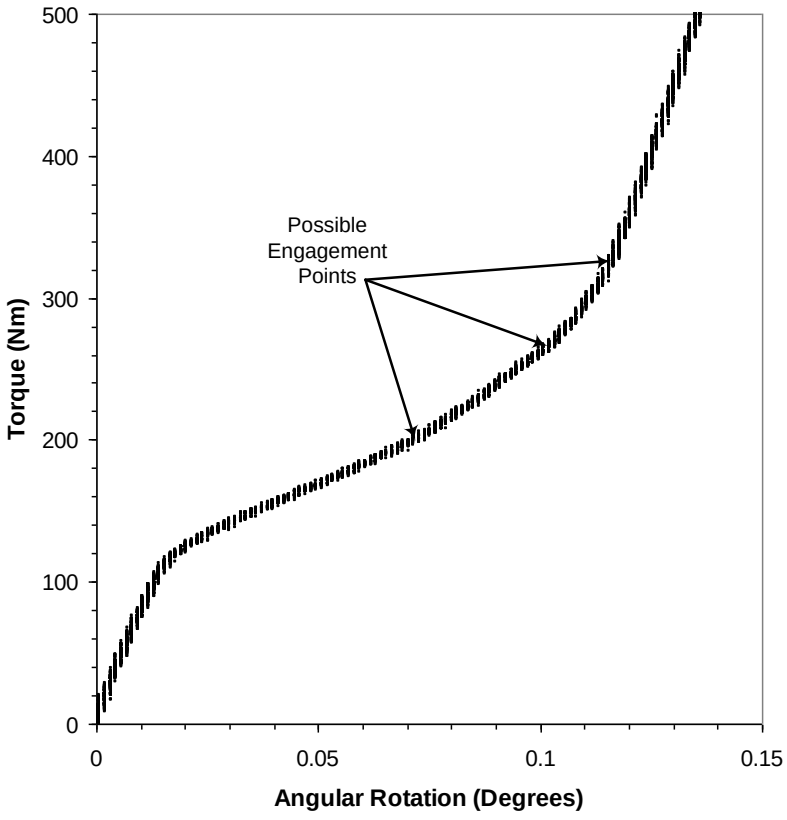

Figure 1-6 Results of a spline coupling stiffness test performed by sponsor

Previous work assumed the clearance variation to be normally distributed based on the fact that the clearance represents the accumulation of several variations in the two components. Such random errors do not produce repetitive patterns or clusters. Purely sequential tooth engagement means as each tooth engages, the slope is incrementally increased. However, clustered engagement means multiple teeth engage simultaneously, and then the slope would increase by a factor proportionate to the number of teeth to engage as shown in Figure 1-7.

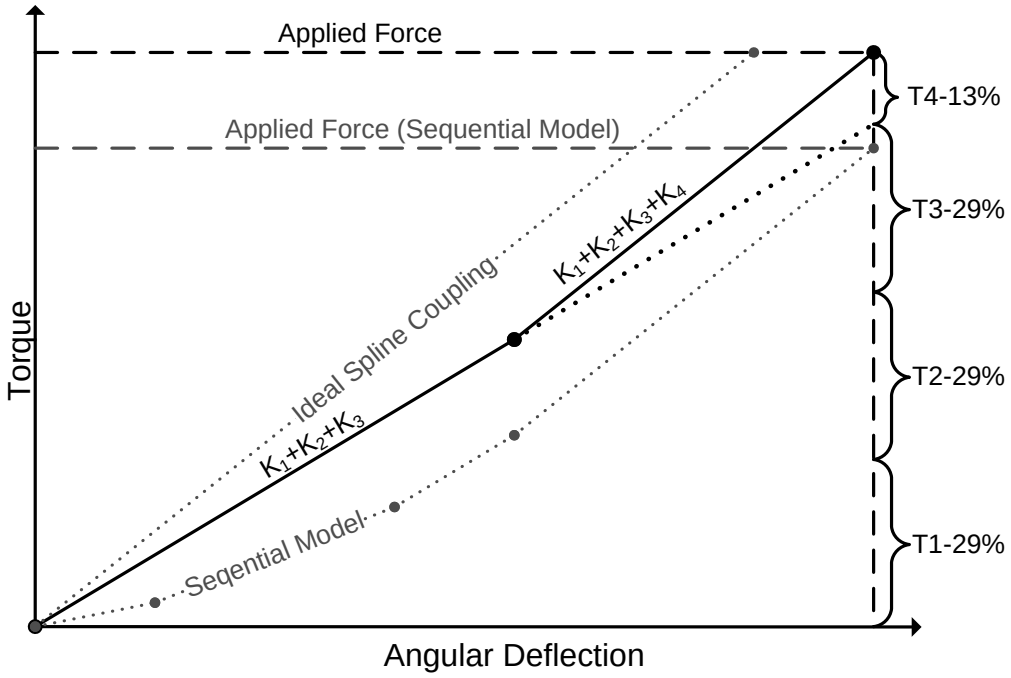

Figure 1-7 Engagement profile when multiple teeth engage simultaneously

It is possible that the lab results are exhibiting both sequential and grouped tooth engagement. A better understanding of exactly where and when each tooth pair engages will reveal potential patterns and aid in understanding their source.

1.3 Thesis Objectives

This research has concentrated on finding and understanding variation and error patterns associated with involute splines. Potential sources of error patterning may be found in cutting tool design, manufacturing methods, and tool sharpening. This research involves a detailed analysis of spline measurement data taken from an internal and external involute spline, which was tested by the industrial partner. This research also focused on identifying and understanding how tool design and the manufacturing processes, like hobbing and broaching, can contribute to error patterns on generated splines. In order to investigate error patterns in spline manufacture, the following steps were performed:

1. Examine internal/external spline variations at roots and tips
2. Examine internal/external spline variations along flanks
3. Examine spline coupling contact location and variation
4. Determine tooth stiffness values for mating pairs of spline teeth
5. Create an analytical tooth engagement curve
6. Compare and contrast analytical results with experimental results
7. Analyze the hobbing process to identify error sources.
8. Create a CAD simulation of the basic hobbing process
9. Examine how hob errors are transferred to the spline.
10. Evaluate the causes of error patterns and possible disadvantages or benefits
11. Make recommendations for process improvements
12. Interpret experimental test results
13. Recommend alternative experimental setups

The principal challenges in this research were:

1. Analyzing and extracting useful information from inspection data
2. Identifying sources of spline variation
3. Comparing and contrasting experimental and analytical results
4. Understanding and representing the complex geometry of the hobbing process.
5. Drawing conclusions as to error sources and recommendations that mitigate them.

By identifying and better understanding error patterning, unique spline designs may arise, which mitigate error or use error patterns to increase teeth engagement and decrease tooth loads in spline couplings.

1.4 Scope Delimitations

This research was limited to the study spline couplings composed of internal and external splines (see Figure 1-8) with involute profiles and the associated tools and processes used to generate them. The focus on involute spline couplings was done with the intent of understanding process errors and their impact on tooth engagement. Furthermore, this research was confined to two-dimensional analysis, with only basic consideration of three-dimensional effects.

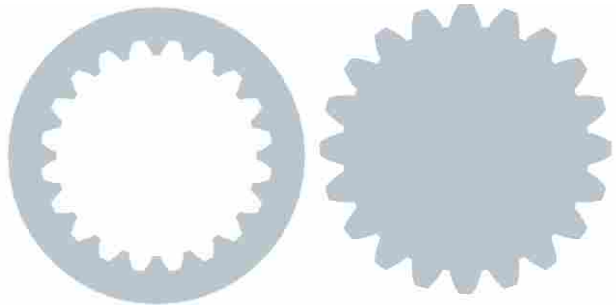

Figure 1-8 Two-dimensional view of internal spline and external spline

Applications of spline couplings may include transmission assemblies and multi-disk brakes, but the theory may be extendable to other applications that employ similar designs. Of particular interest to this research was the presence and source of patterns; therefore, random errors and outliers were only given limited attention.

Chapter 2 Background Research

To better understand error patterning in splines, a review of basic literature associated with involute geometry, splines and spline applications, hob geometry and the hobbing process is necessary, all of which involve complex geometry, mathematics, and process technology.

2.1 Involute Curve

Like gears, spline teeth typically have an involute profile. The involute of a circle is the curve that is described by the end of a line which is unwound from the circumference of a circle [2]. Involute can also be defined as follows: if the base circle is fixed, and a rigid bar AD rolls without slipping on the base circle, then the path followed by point A is an involute [4].

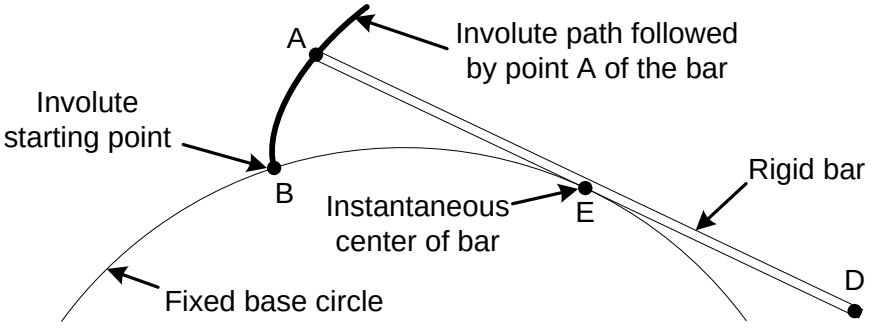

Figure 2-1 A rigid bar rolling on a fixed cylinder [4]

A basic overview of typical geometry used in defining an involute is shown in Figure 2-2 [14]. The involute curve is generated by the taut line ρ that is unwound from the base circle with radius R_b (see Equation (2-1)). The radius vector r begins at the base circle center C and extents to the end of the taut string at point p.

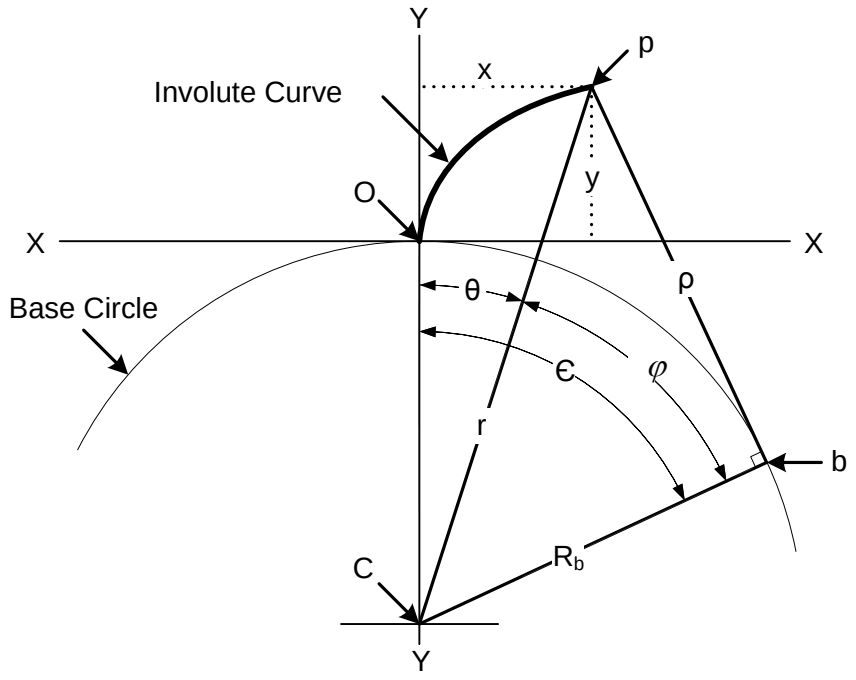

Figure 2-2 Generating an involute curve from a base circle [14]

The roll angle Є is the sum of the vectorial angle θ, and the pressure angle φ which can be used in determining the x, y coordinates of p at any point along the involute curve as defined in Equations (2-2) and (2-3).

$$\rho = R_b(\varphi + \theta) \tag{2-1}$$

$$x = R_b \sec\varphi \sin\theta \tag{2-2}$$

$$y = R_b(\sec\varphi \cos\theta - 1) \tag{2-3}$$

In gears, the involute is a practical design that is used in order to generate conjugate action, or smooth continuous rotation between mating gears, while maintaining a constant pressure angle, for smooth transmission of torque [12]. Though conjugate action is not exhibited in splines, the involute profile is the predominant spline form because they are stronger than straight sided splines and are easier to cut and fit [8]. Involute splines are also readily manufactured with existing techniques, like hobbing and broaching for external and internal splines, respectively.

2.2 Splines and Applications

Splines are typically designed with shorter teeth and larger pressure angles than standard gears in order to carry higher loads. The standard pressure angles for involute splines are 30, 37.5 and 45 degrees, whereas gears typically utilize pressure angles of 14.5, 20, or 25 degrees [1].

Splines are a special class of gears that do not engage in conjugate action or smooth continuous motion, rather teeth in a spline coupling remain fixed relative to each other. Internal and external splines are designed to allow a shaft to engage with a hub over the full circumference. Unlike gears, the point of contact between mating spline teeth remains constant and multiple teeth (ideally, all teeth) engage in order transmit torque; therefore, splines are ideal for applications involving high torque loads. For example, spline couplings are used in braking applications for large industrial vehicles, like the huge dump trucks used in mining operations. Figure 2-3 is an exploded view of such a braking application, which uses two sets of spline couplings in order to provide a braking force. The inner set of spline couplings contains the shaft and the friction plates,

while the outer set of spline couplings is comprised of the separator plates and the hub. The hub coupling remains fixed, while the shaft coupling rotates.

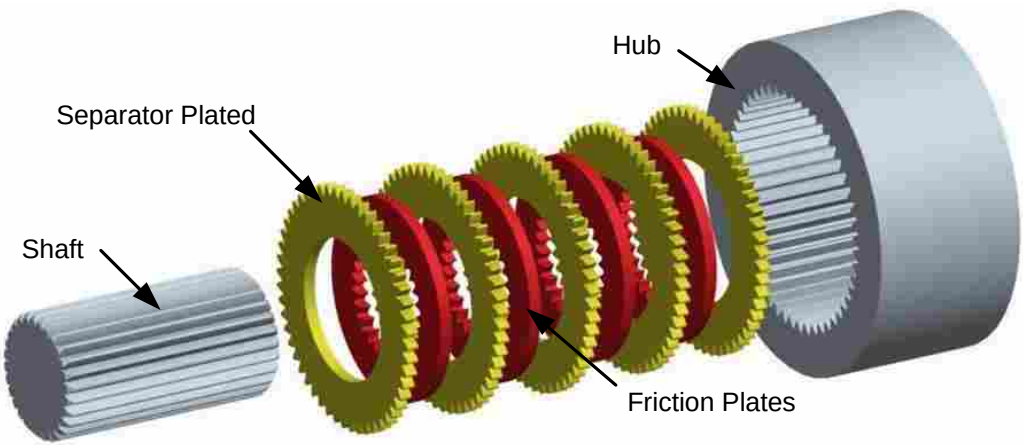

Figure 2-3 Industrial braking system using internal and external splines

The hub and shaft spline couplings are comprised of internal and external splines, which transfer torque without any slipping. Prior to applying the brakes, the shaft coupling rotates freely inside of the hub coupling. When the brakes are applied, the separator plates are squeezed together, applying pressure to the rotating friction plates, creating the braking force needed to stop the rotation of the shaft.

An extreme application like industrial brakes is a key candidate for using error patterning in spline couplings to increase tooth engagement. Patterning may allow for sets of teeth to simultaneously engage, rather than one tooth at a time, thereby reducing the total load carried by any single tooth. If we can better understand sources of error patterning in splines, it may be possible to better design spline couplings for such high load applications.

2.3 Spline Coupling Overview

The study of tooth engagement in involute spline couplings requires an understanding spline geometry and terminology. Typical terminology used is describing spline geometry is shown in Figure 2-4. On the external spline, whose teeth face outward, the major and minor diameters refer to the tips and roots of the teeth respectively. On the internal spline, whose teeth face inward, the major and minor diameters refer to the roots and tips respectively (See Appendix A for spline terminology definitions).

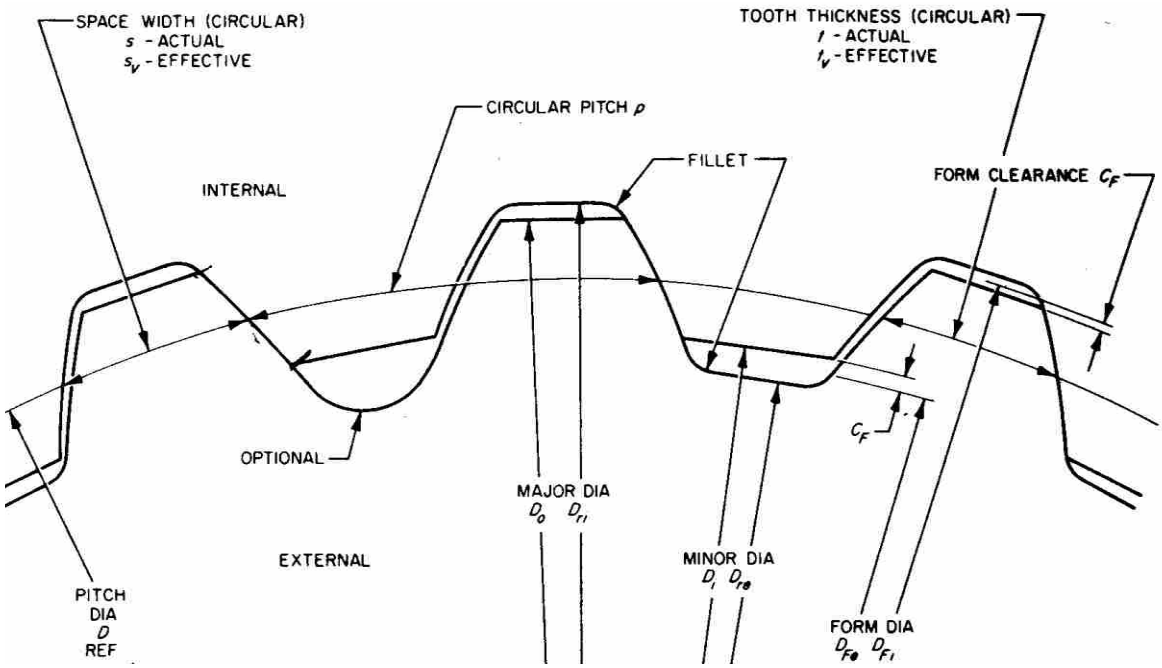

Figure 2-4 Typical terminology used for internal and external splines [1]

2.4 Categorizing Error

Previous work has studied common errors associated with spline geometry and grouped these errors into categories [15]. Some of the common errors associated with splines, in two dimensions, are shown in Figure 2-5.

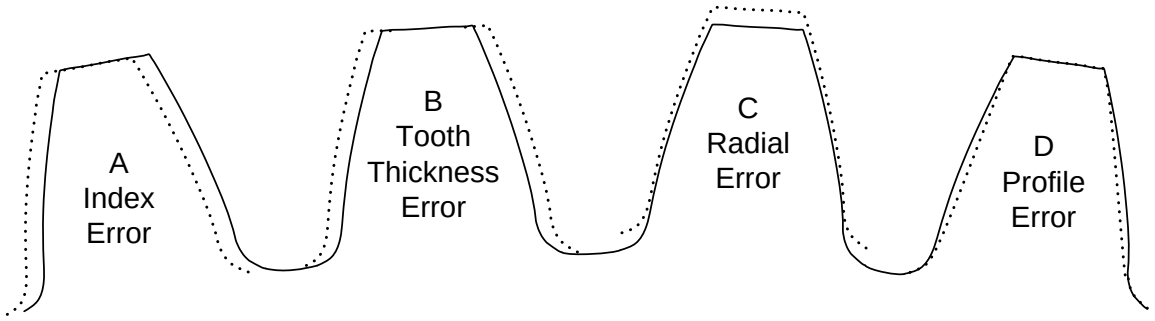

Figure 2-5 True involute profile (solid line) and four error categories (dotted line)

Understanding errors and error sources is important in spline coupling analysis in order to understand tooth-to-tooth clearance variation and engagement sequences and patterns. Due to complex tooth geometry and very small errors, it is challenging to identify and analyze spline tooth variation and the resulting tooth-to-tooth engagement. For example, in order to gain the resolution necessary to detect tooth profile errors, very large amounts of data need to be gathered. Furthermore, in order to test tooth engagement in spline couplings, very sensitive equipment must be used and great care must be taken in the experimental setup and execution.

2.5 Modes of Deflection

Deflection is another area of significant importance in understanding tooth engagement in spline couplings. As two teeth engage, each tooth begins to deflect as the load increases. How each tooth pair will deflect is important to understand in order to know when the next tooth pair will engage. Previous research performed by DeCaires has studied three modes of deflection: shear, bending, and contact (see Figure 2-6). Of the three modes of deflection, contact deflection is insignificant and is therefore ignored.

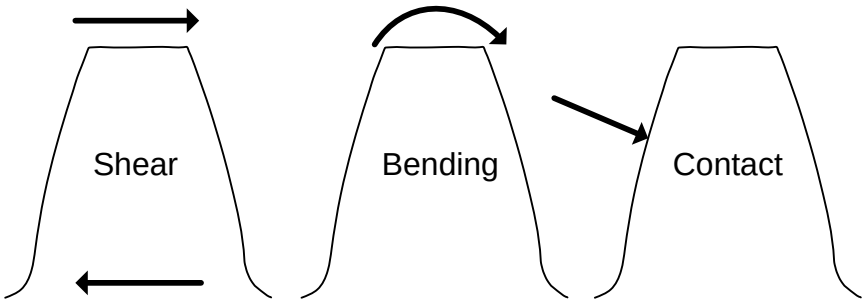

Figure 2-6 Three modes of tooth deflection

2.6 Tooth Engagement Models

Previous work in the area of tooth engagement analysis has been performed by Brian DeCaires and Janene Christensen, who helped develop the STEM and ProTEM analytical models [7]. DeCaires provided a model for tooth stiffness, which is critical for tooth engagement predictions. He also analyzed stress and deflection due to bending, shear, and contact loads. Furthermore, stress and deflections were verified using a fine mesh finite element model. He found that contact stresses and deformation could be neglected in predicting tooth behavior. DeCaires also developed a spreadsheet model for

predicting tooth engagement statistically and found close agreement with finite element and Monte Carlo simulations. Furthermore, he was the first to observe possible error clustering from Caterpillar's experimental results. This previous work has provided motivation to further investigate error clusters and error patterning which may result from the hobbing process. Previous models do not account for error patterns, but aided in providing the foundation upon which this research on error patterning is based.

Chapter 3 Commercial Spline Tests

In order to better understand what happens when spline coupling teeth engage, an experiment with sample production splines was conducted. The industrial partner for this research performed precise lab measurements on a spline coupling assembly under load in order to detect sequential tooth engagement that results from tooth-to-tooth variations. By comparing physical results with analytical results and understanding their similarities and differences, better models and experiments for future tests may be devised to further the understanding of tooth contact in spline couplings.

3.1 Experimental Setup

The lab test was performed with a production hub (external spline) and a mating frictionless brake disc (internal spline) with specifications described in Table 3-1.

Table 3-1 Specifications of hub and disc used in experimental setup

	Hub	Disc
Number of teeth	65	65
Normal Diametral Pitch	8	8
Normal Module	3.175	3.175
Pressure Angle	14.5°	14.5°
Pitch Diameter	206.375 mm	206.375 mm
Base Diameter	199.801 mm	199.801 mm

The purpose of the experiment was to create a torque-deflection curve by measuring the torque applied to a spline coupling and measuring the resulting angular deflection. A photograph of the experimental setup is shown in Figure 3-1. The setup was composed of a rotary actuator, various adaptor plates and bolts, and a spline coupling. The shaft of the external spline in the setup was welded to an adaptor plate, which was fastened with eight bolts to a 200,000 in-lb rotary actuator, (Note: the maximum torque applied was 17,701 in-lb or 2000 N-m).

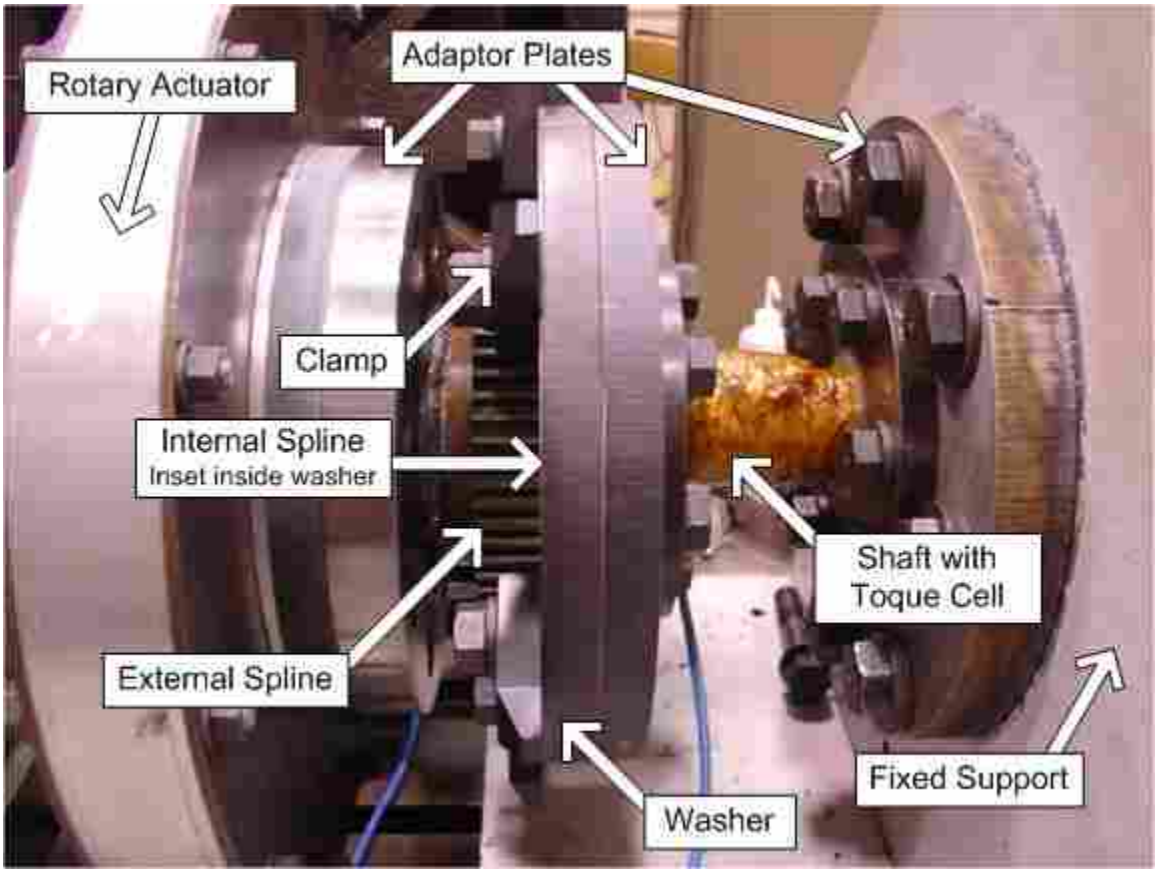

Figure 3-1 Photo of experimental setup to test tooth engagement

The internal spline (brake disk), was fastened against a washer plate with six toe clamps, which in turn were fastened to an adaptor plate (see Figure 3-2). The adaptor plate was bolted to a flanged shaft with a torque cell. The shaft was bolted to a fixed support using another adaptor plate. The torque cell had the capacity and resolution needed for reading the maximum torque administered by this test. The torque was applied by the rotary actuator and was measured by the torque cell, while the corresponding deflection was collected from the rotary actuator via a MTS 407 controller. Special care was taken to ensure that the internal spline was concentric with the external spline prior to fastening the toe clamps. The complete assembly appears to be adequately stiff.

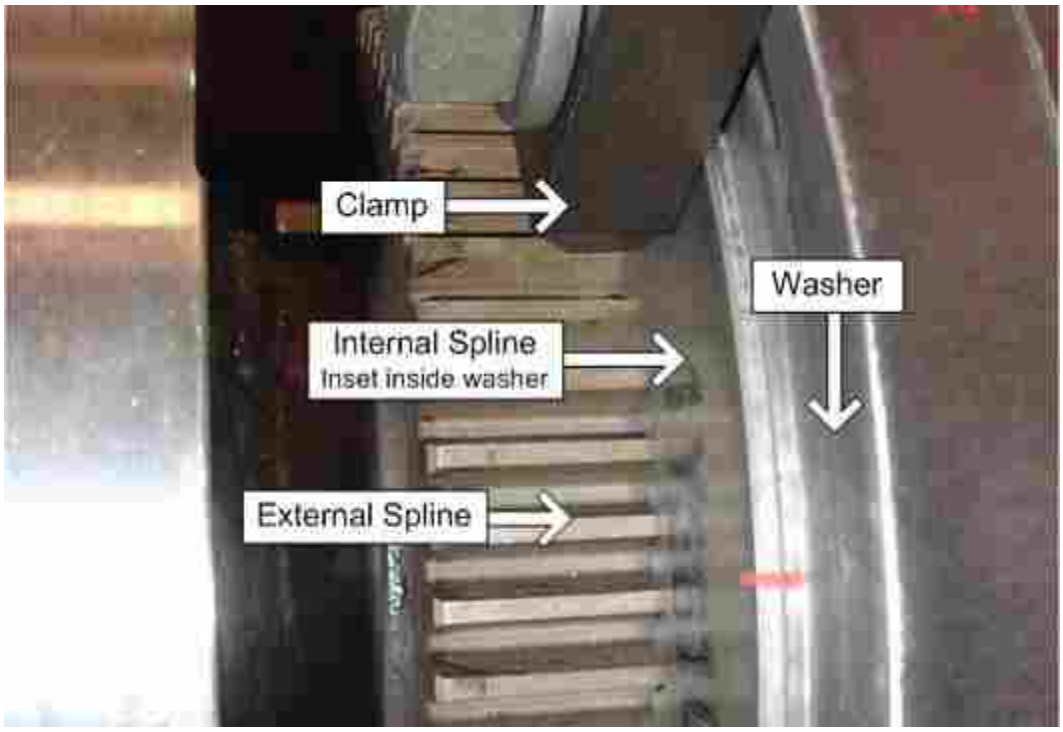

Figure 3-2 Photo showing internal and external spline in experimental setup

After a test was run, the coupling assembly was reconfigured by rotating the disc 45 degrees and then re-testing. This process was repeated for three different configurations. After the experiment with the first disc was completed (in three configurations), another disc was tested in similar fashion.

3.2 Experimental Results

The results from the three configurations that were tested with Disc 1 and Disc 2 are shown in Figure 3-3 and Figure 3-4 respectively. The results from the Disc 1 experiment reveal interesting behavior. There are incremental slope changes. For example, in the red and green tests, when the torque is first applied, there is a relatively steep initial curve, which flattens out at about 0.01 degrees. Then around 0.09 degrees, the slope begins to increase slightly, until the deflection reaches about 0.12 degrees, at which time the slope becomes steep, like it was in the beginning. While the red and green path coincide very closely, the black path differs in that it starts out shallow, transitions to a steep slope earlier, and the load and unload path appear the same; however, the black path maintains slopes that are comparable to the red and green paths.

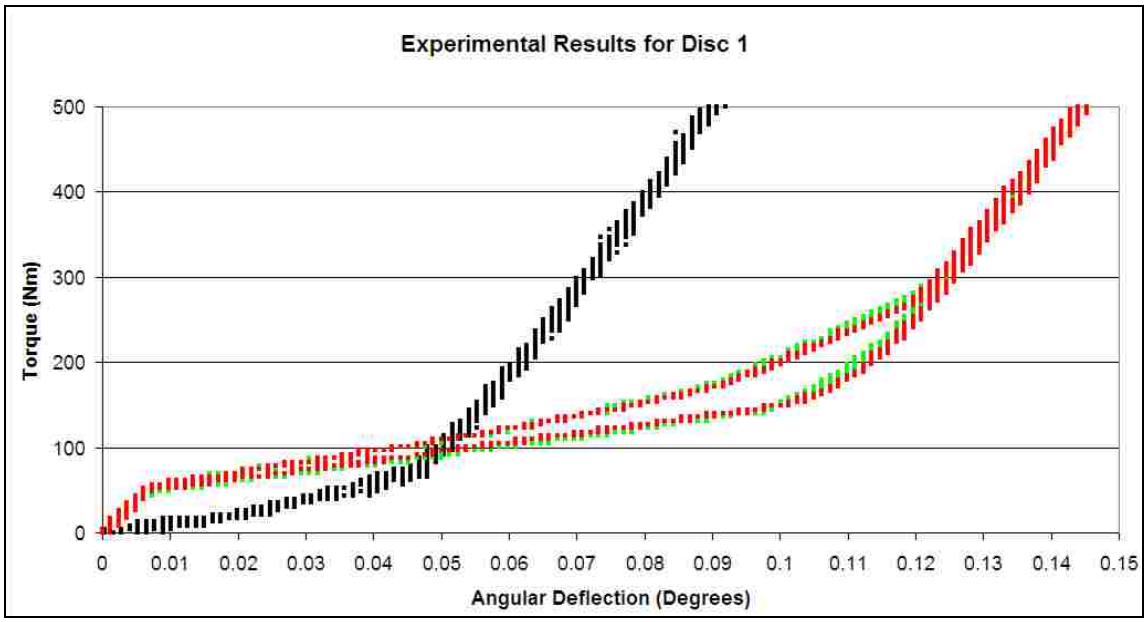

Figure 3-3 Disc 1 results for three configurations

It can be noted from the torque-displacement graphs that the data appears as a series of data points in short vertical bars. These vertical bars are a function of the measurement process and not an actual phenomenon of tooth engagement. The clusters are a result of a one-to-many data collection process, where multiple torque measurements are recorded at the same angular deflection point due to the resolution of the measurement equipment and the sampling rate. The angular data is recorded at approximately 0.00122 degree increments, this permits each tooth profile to be compared to its theoretical profile.

Once the maximum torque was reached, the assembly was gradually unloaded and instead of following the same path, a new return path was created that lies below the load path. This demonstrates a hysteresis phenomenon, in which the loading and unloading paths differ (Note: the black data set in Figure 3-3 does not display significant hysteresis).

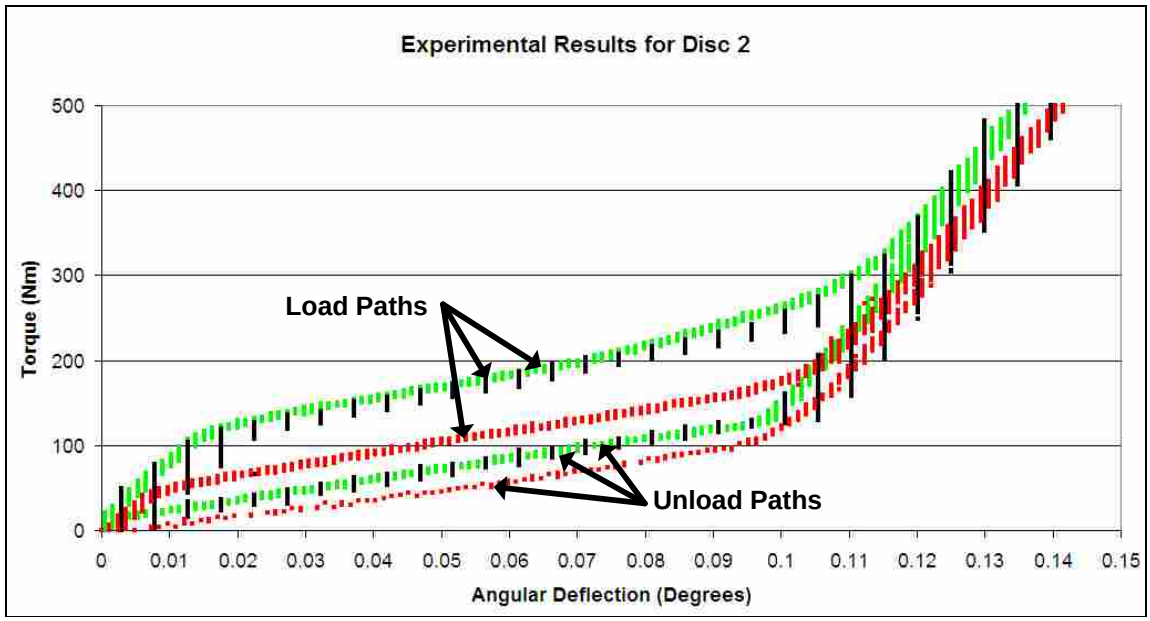

Figure 3-4 Disc 2 results for three configurations

The results from the experiment on Disc 2 are similar to those of the Disc 1 experiment in that they again show that the loading and unloading paths are different, and the shape of all three configurations is consistent. Also, the initial steep slope is followed by a shallow slope, and then concludes with approximately the same steep slope that it began with. It is also noted that the angular resolution of the black curve in Figure 3-4 is different from the green and red curves (about one fifth the resolution).

In order to better understand these results and interpret the behavior described by these graphs, a detailed analysis is employed in Chapter 6 to provide additional models for comparison.

3.3 Measurement Data

In addition to the experimental results obtained from the industrial partner test, profile inspection data was collected on the hub and Disc 2. Disc 1 was not measured. Using precision inspection, the spline profiles were measured (see Appendix C for sample output from the inspection process). Although the actual resolution is unknown, profile measurements were recorded to the nearest 0.001mm at 0.00122 deg. increments. The 2-D scans of the splines resulted in 26,000 and 25,695 data pairs for the complete profile of a 65 tooth internal and external spline, respectively. This inspection was performed both before and after the experimental testing in order to assess any changes that may have occurred to the spline profiles during testing. From this data the industrial partner determined that no noticeable deformation had occurred to the splines as a result of testing.

Using the measurement data, the tooth-to-tooth clearances were calculated for all assembly configurations. An analytical model was created to describe the tooth-to-tooth clearance variation and simulate teeth engagement for each configuration. These analytical results were then compared to the experimental results to determine differences and similarities, particularly, the occurrence and steepness of the incremental changes in slope.

Chapter 4 Internal & External Spline Analysis

Greater understanding of the error associated with the assembly was gained by better understanding the errors associated with individual components; therefore, the spline measurement data taken (before testing) was analyzed in order to find error patterns that might be associated with each spline. Prior to examining the mating involute profiles, a careful analysis was performed on the variations associated with the roots and tips of the involute splines. Though the roots and tips of splines do not contact during engagement, they may reveal eccentricity variations and patterns that also affect contact at the tooth flanks.

Understanding the variation in the roots and tips is even more important in this study because the manufacturing method and tools are unknown; therefore, for example, an understanding of roots, tips, and flanks can aid in assessing whether or not a topping or non-topping cutting tool was used.

The analysis of the measurement data that described the splines was separated into two parts: 1) radial location of the tooth root and tips and 2) angular variation of the contact profile. For a theoretically perfect gear, the radial distance from the center of the spline to each individual tooth tip/root will be exactly the same, no matter which tooth is measured. However, due to manufacturing variations the radial distance to each tooth tip/root location will vary.

4.1 External Spline Errors

The external spline analysis was performed on the data that was gathered from the spline inspection prior to testing (25,695 x, y data pairs with fixed coordinate origin). The spline data was plotted and each root and tip was indexed from 1 to 65 as shown in Figure 4-1.

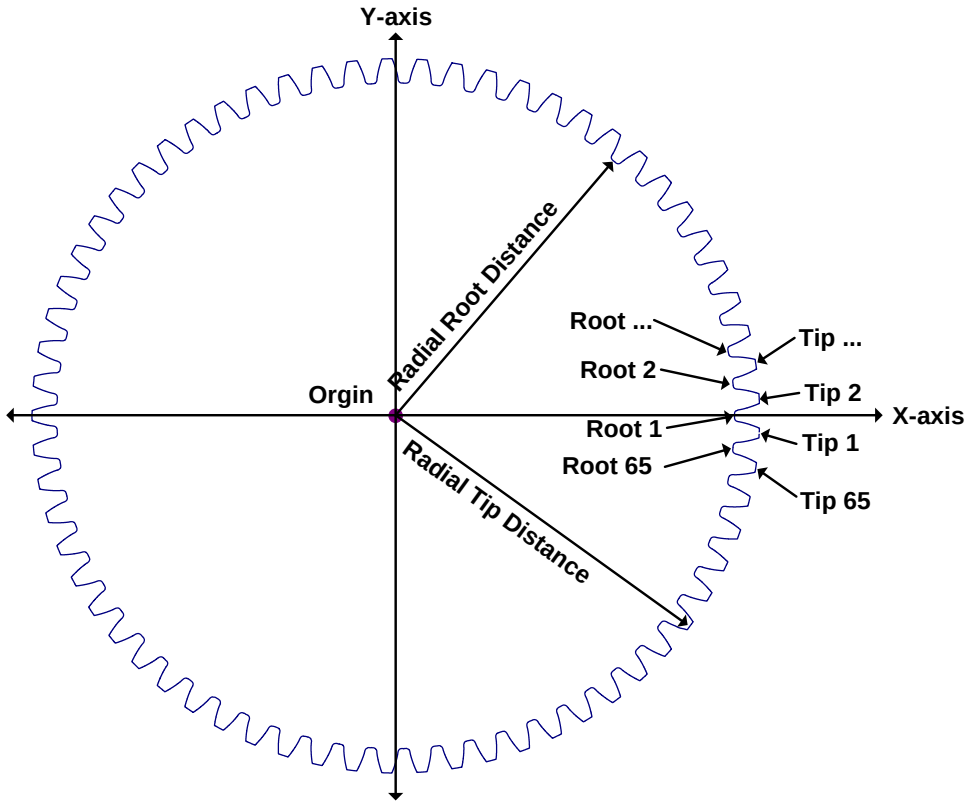

Figure 4-1 Data plot of inspection data from the external spline

According to the spline specifications, the theoretical radial root and tip distances should be 100.15 and 107.38 mm respectively. Any measured variation from the specifications should be random (assuming ideal manufacturing capabilities). To

determine the actual root and tip location the data was transformed from Cartesian to polar coordinates using Equations (4-1) and (4-2)

$$r = \sqrt{x^2 + y^2} \tag{4-1}$$

$$\theta = a\tan 2(x, y) \tag{4-2}$$

Once in polar coordinates, a spreadsheet was developed to find the average of the smallest radial values on each root (five values were used in the average); the result was a single radial distance to represent the location of each root as shown in Figure 4-2.

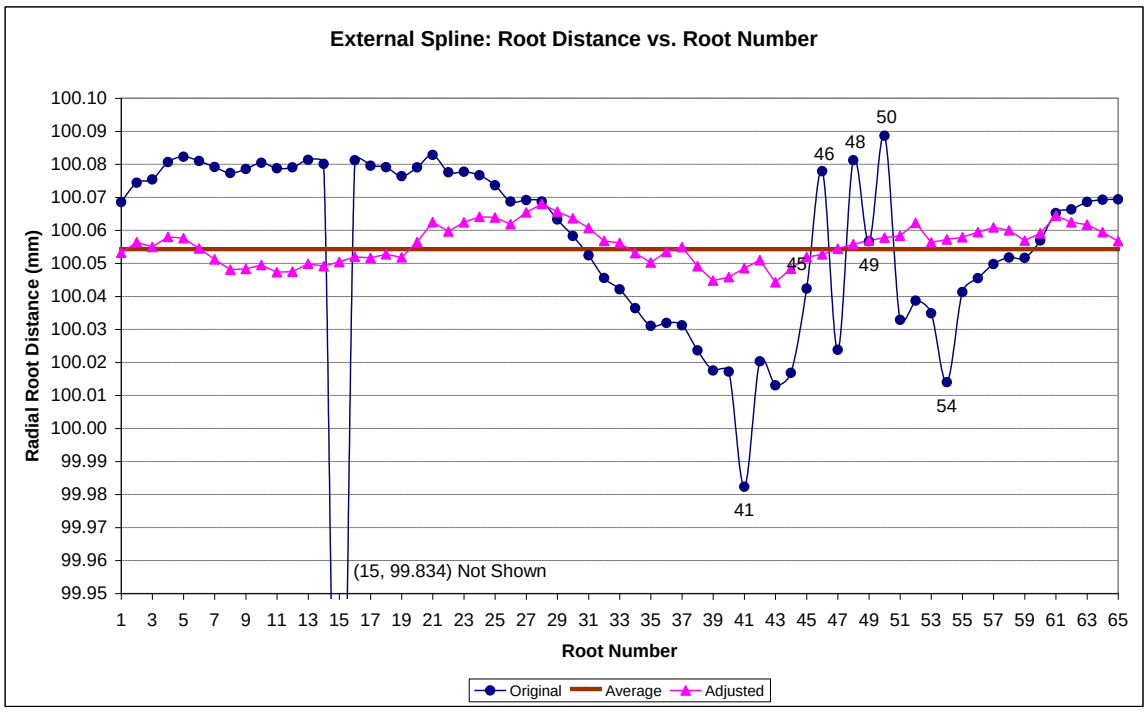

Figure 4-2 Average distance from the root to the center of the spline

The results shown in Figure 4-2 show that the average distance from the spline center to the root is 100.055 mm and display a single wave-like pattern (with the exceptions of points 15, 41, 45, 46, 48, 49, 50, and 54). Next, a test was performed to see

if this wave-like pattern was due to eccentricity in the manufacturing of the roots. To test for eccentricity, the root radial values and corresponding tooth locations were converted from polar back to Cartesian coordinates using Equations (4-3) and (4-4).

$$x = r\cos\theta \tag{4-3}$$

$$y = r\sin\theta \tag{4-4}$$

Once in Cartesian coordinates, an optimization routine was setup to find an X and Y shift that would minimize the total error between the mean radius and each of the 65 individual tooth radii (this was done by ignoring the exception values mentioned earlier). The result was a shift of -0.0167 mm in the X direction and -0.0267 mm in the Y direction. The data was then converted back to radial coordinates and plotted as a function of tooth number and is also shown in Figure 4-2. This adjusted center resulted in a significant decrease in the variation from the mean, suggesting that eccentricity was a significant contributor to variation in the setup and manufacturing of this spline.

A similar analysis was performed on the radial distance to the tips of the teeth on the external spline and the results are shown in Figure 4-3. Again, a distinct single wave-like pattern is apparent in Figure 4-3, which shows the smaller radial values occurring in the middle of the graph and higher radial values occurring on the sides. Using the optimization routine discussed earlier a new (X, Y) center that minimizes the error was found to be located at: (-0.0584, 0.0170) mm.

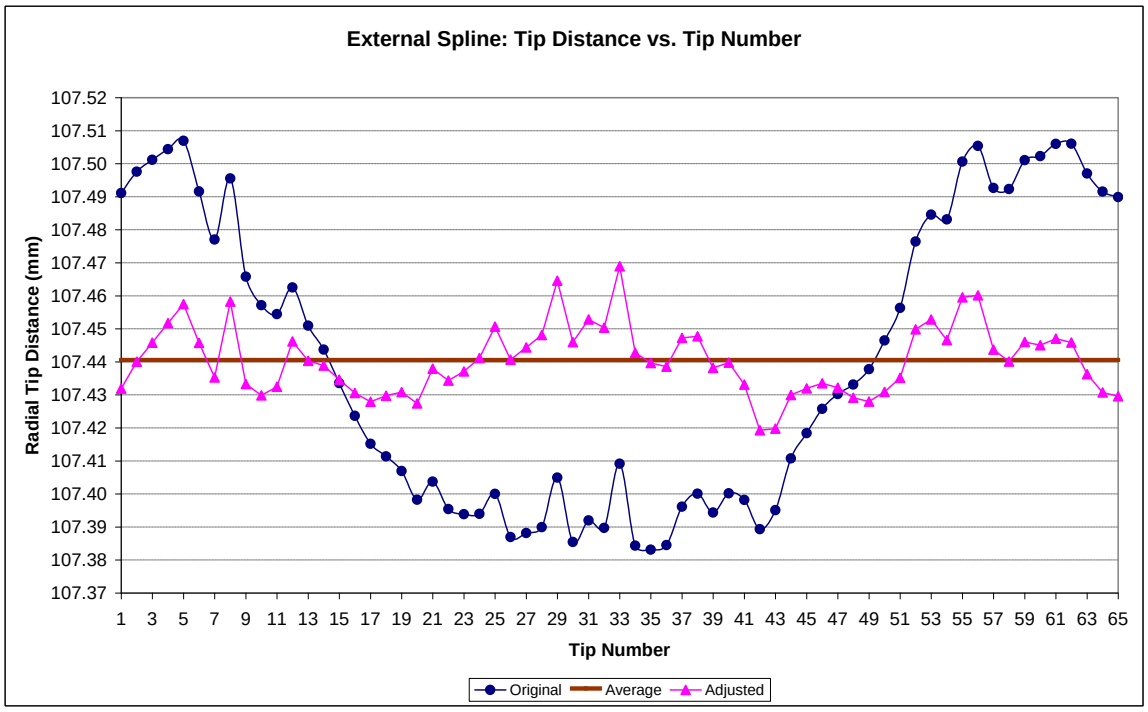

Figure 4-3 Average distance from the tip to the center of the spline

It should also be noted here that the optimized center value for the external root analysis of (-0.0167, -0.0267) does not match the optimized center value for the external tip analysis, nor do the two waves in Figure 4-2 and Figure 4-3 line up with each other. These observations will be considered in greater detail in the external spline manufacture section.

4.2 Internal Spline Errors

The tips and roots of the internal spline were also analyzed in the same way as the external spline (the internal spline is described by 26,000 X, Y data sets). The analysis of the root location is shown in Figure 4-4.

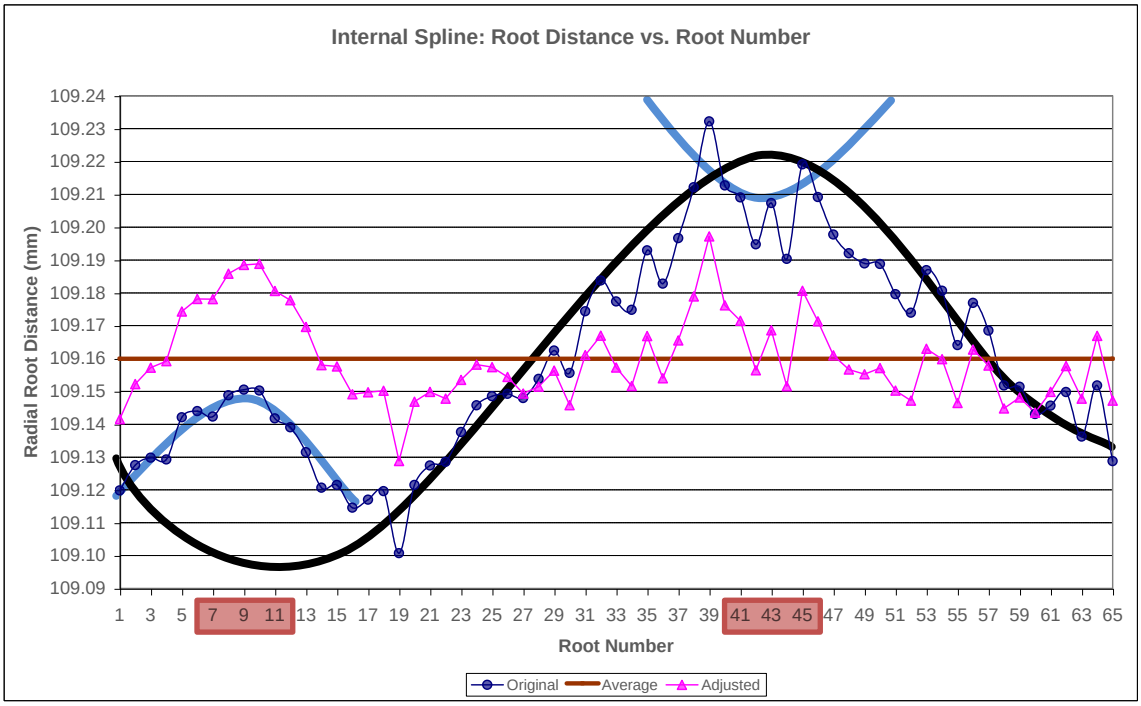

Figure 4-4 Internal spline root analysis showing two wave-like patterns

This analysis also shows a wave-like pattern; however, there appears to be two wave patterns. These patterns are marked in Figure 4-4 and are identified by looking at the peaks and valleys of the plot and finding a corresponding peak or valley 32 or 33 teeth away (32.5 teeth equals 180 degrees).

It can be seen from Figure 4-4 that valley of the black wave is about 180 degrees away from the peak of the black wave. If the peak of the blue wave were a valley 180 degrees away it would lower the peak of the black wave. A tip analysis was also performed on the internal spline, which revealed random radial variation of tip location as shown in Figure 4-5.

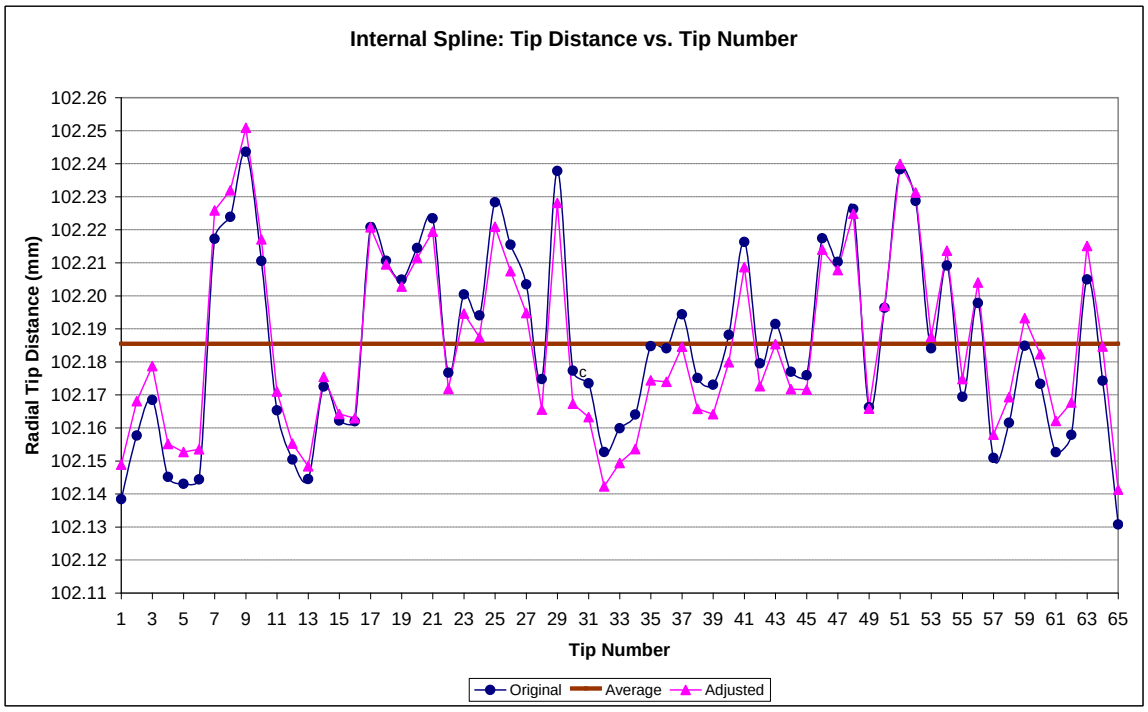

Figure 4-5 Internal spline tip analysis

The tip analysis profile for the internal spline is unique in that the radial values appear to be randomly distributed about the mean and no strong wave-like patterns are apparent. Furthermore, when the tip positions where optimized to find a new center the result showed very little if any improvement in reducing the radial tip distance variation.

4.3 Least Squares & First Difference Comparison

Previously, a least squares method was used to find the eccentricity associated with the spline tip and root locations. By using a least squares optimization procedure a new center can be found and the strong wave patterns can be minimized. Another method of removing the wave-like pattern is by using a differencing approach. A first differencing approach is often using in time series data in order to remove trends [13].

Our data set is unique in that it begins and starts in the same place therefore a first difference approach would remove eccentricity error. This approach takes the radial value for tooth #1 and subtracts it from tooth #2 then takes the radial value for tooth #2 and subtracts it from tooth #3 and so forth. The result should be randomly distributed values about zero. The results from the least squares method and the first difference method are shown in Figure 4-6.

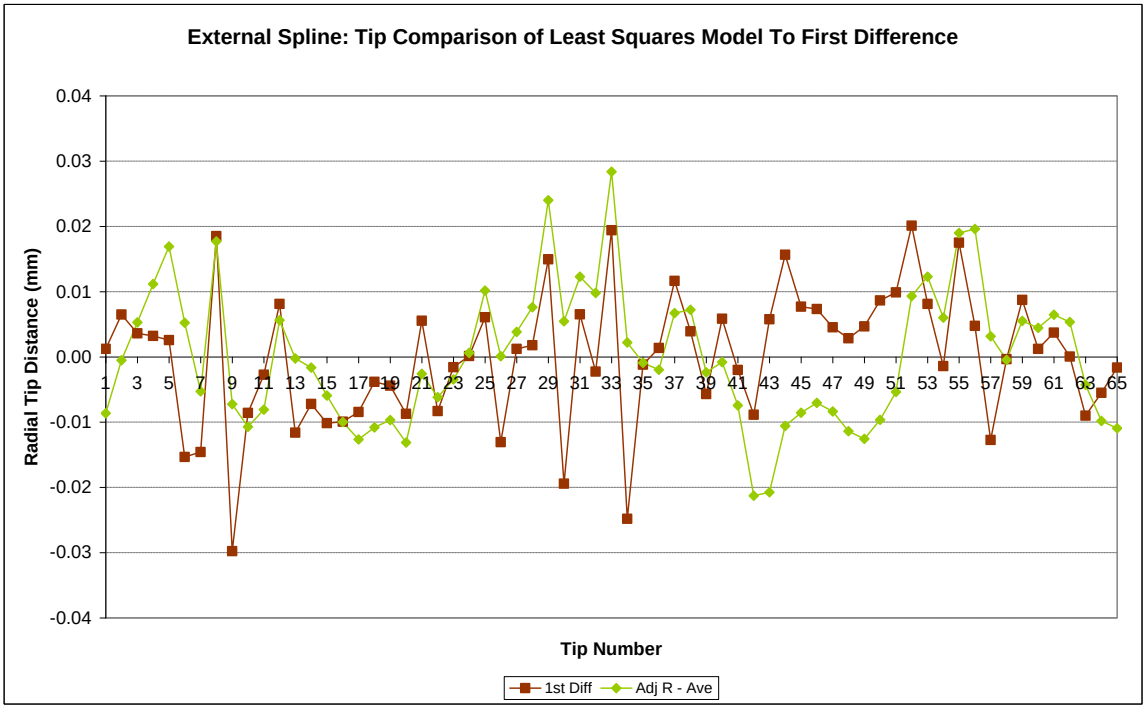

Figure 4-6 Comparison of least squares to first difference in eliminating eccentricity

The results shown in Figure 4-6, comparing the least squares method to the first differencing method was also performed on the external roots/tips, internal roots/tips of the internal and external splines; in each case the first difference and least squares

methods both provided similar results. Though both methods provide similar results, the first differencing method is much simpler and does not require solvers.

4.4 Summary of Results

The results of the spline roots and tips analysis are summarized in Figure 4-7. Though the y-axis values on each of the four figures are different the scale and total range of 0.015mm is the same, making it easy to compare the four graphs. The following is a summary of the observations from these graphs:

1. The external spline shows wave-like patterns at roots and tips (A and B).
2. The wave-like patterns on the external spline are not aligned (A and B).
3. The external roots display about multiple deviations from the wave pattern (B).
4. The internal spline displays a dual wave-like pattern at the tips (C).
5. The internal spline has random variation at the roots (D).
6. Patterned variations in A, B, and C are notably reduced using least-squares or first differencing.

(A) External Tips (C) Internal Tips

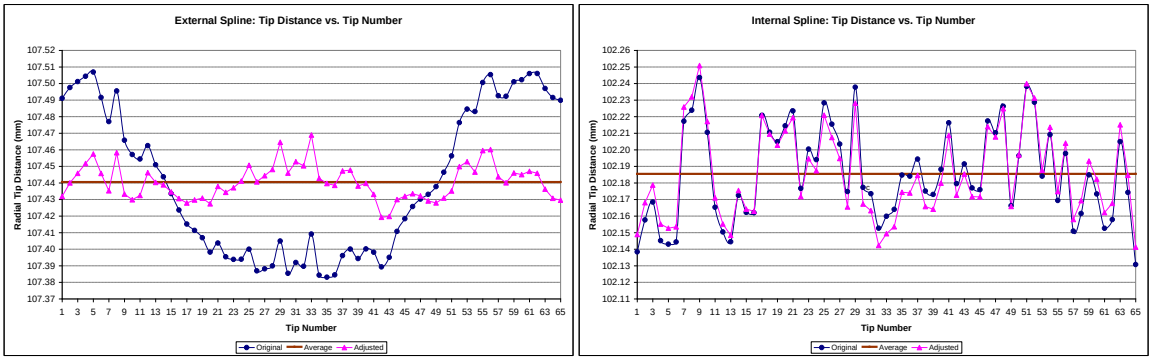

(B) External Roots (D) Internal Roots

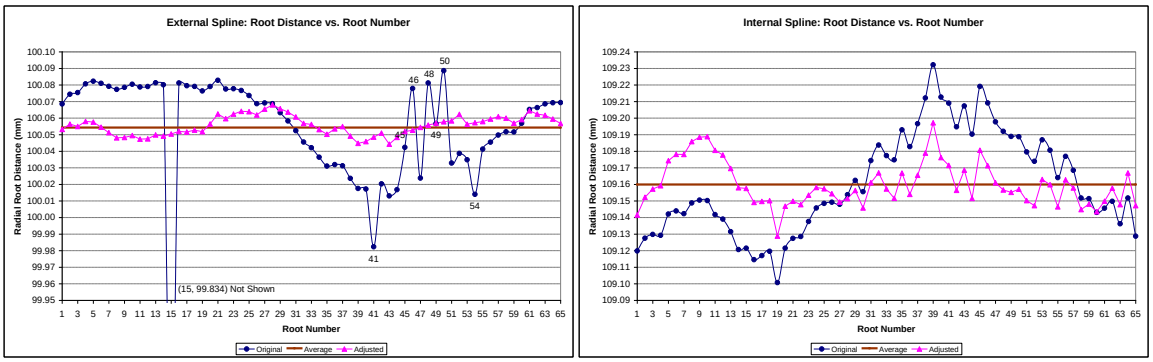

Figure 4-7 Summary plots of spline analysis

The plot shown in Figure 4-8 summarizes the four newly found centers that best corrected for the eccentricity found in the measurement data of the tips and roots. This plot shows both magnitude and direction of the adjusted centers.

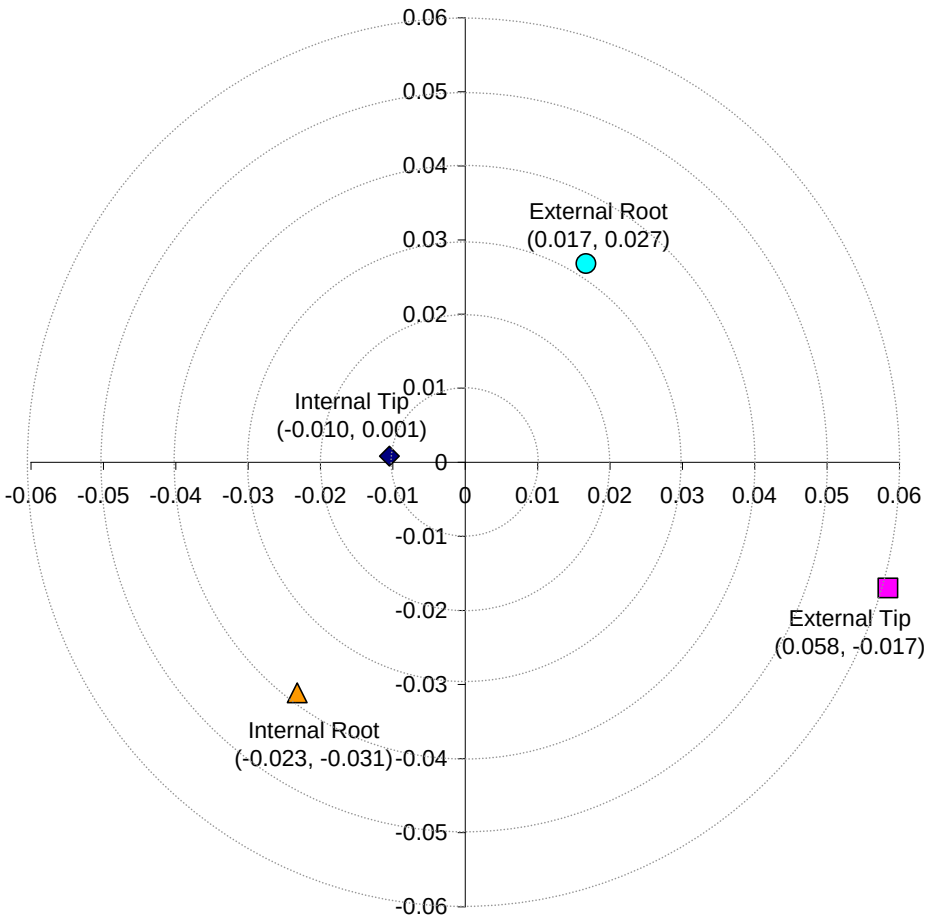

Figure 4-8 Magnitude and direction of eccentricity errors

It can be seen that the external tip and the internal root exhibit the strongest eccentricity error. It is also readily shown that the roots and tips of the external spline are not in the same directions suggesting two different apparent centers.

Chapter 5 Involute Spline Coupling Engagement Analysis

The previous chapter provided an in-depth analysis of the measured variations of the roots and tips of the individual spline teeth in a spline coupling assembly. The analysis revealed an apparent eccentricity due to errors in the machine parts or the test setup. This chapter describes the tooth contact analysis of the internal and external spline in order to better understand when and where tooth contact occurs. The order in which the teeth make contact depends upon the individual tooth errors in each mating pair of teeth. Examining the measured variations in the teeth of the sample test assembly can bring about an increased understanding of assembly performance.

5.1 Overview

Using the measurement data from the internal and external spline components, a CAD model was created from the original data of the spline coupling assembly as shown in Figure 5-1. The CAD model contains the actual measured profile errors. The resulting CAD model in Figure 5-1 shows the spline coupling assembly in the first of 65 possible configurations.

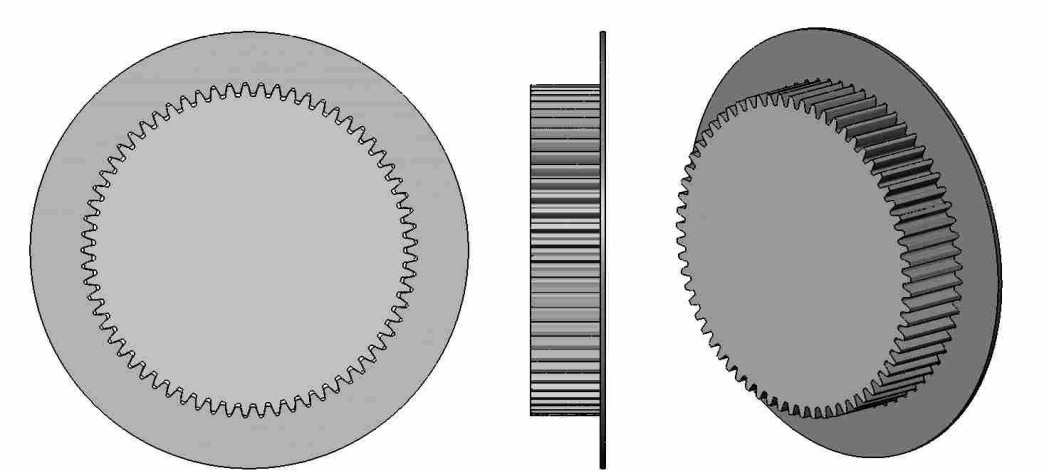

Figure 5-1 3D CAD model of actual profile errors in a spline coupling

The CAD model shows the relative sizes of the internal and external splines. No assembly interferences can be seen in the detailed view shown in Figure 5-2.

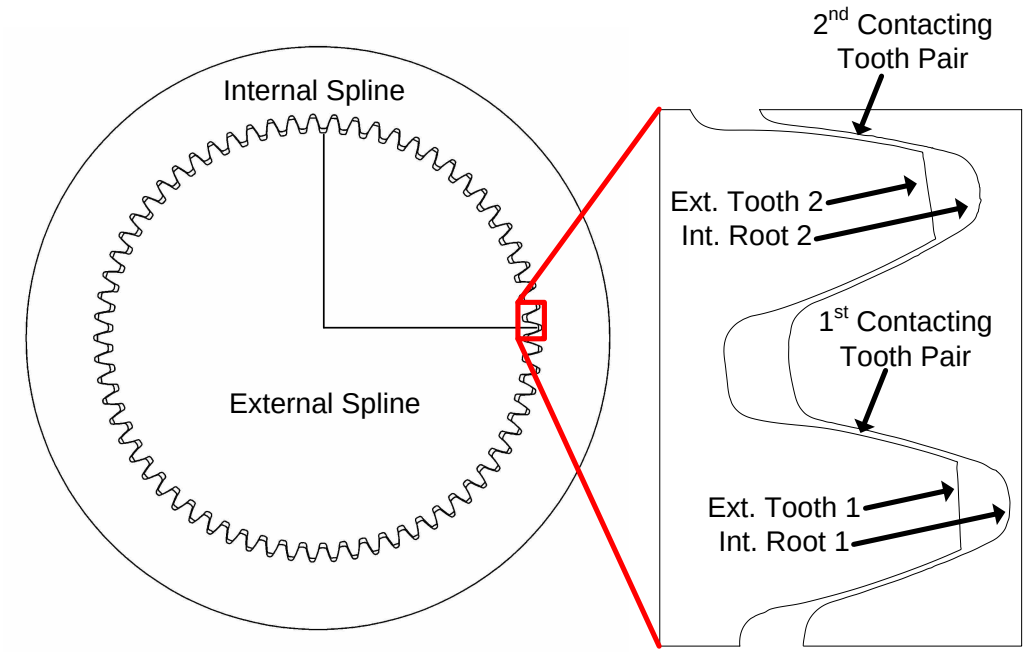

Figure 5-2 CAD plot of spline coupling inspection data and detailed view of tooth pairs

Figure 5-2 shows the CAD model of the spline coupling in its first configuration with the external tooth 1 lining up with the internal root 1, thereby forming the first contact area along the flanks of the mating teeth. With the spline coupling assembled, in this original and first configuration, clearances between each mating pair of teeth can be calculated and these clearances can then be reviewed to see when and where contact will occur and if there are any patterns.

5.2 Tooth-to-Tooth Contact

Prior to calculating the angular rotation required to engage a tooth pair it is important to understand how involute teeth engage. If both involute profiles on the internal and external splines are perfect involutes, then the teeth will engage along the full surface of the involute profile. For mating splines, both mating involutes have the same radius of curvature over their entire length, both having been generated from the same base circle. Therefore, the angular rotation-$\Delta\theta$, required to engage the teeth will be the same anywhere along the involute profiles. With two perfectly mating involute flanks, the arc length of travel between two contacting points increases with radial distance; while, the change in angle ($\Delta\theta$) required to engage the flanks is constant as shown in Figure 5-3 A.

However, teeth profiles are never truly involute, partly due to natural variations associated with manufacturing and partly because the tool and processes used can only approximate an involute profile (see discussion in Chapter 7). Due to this deviation from perfect involute it becomes important to take a very close look at how two mating flanks are really engaging. Figure 5-3 shows a magnified view of two flanks that will engage

when rotated. The x-axis has been magnified by a factor of 10 in order to better display where engagement will first occur.

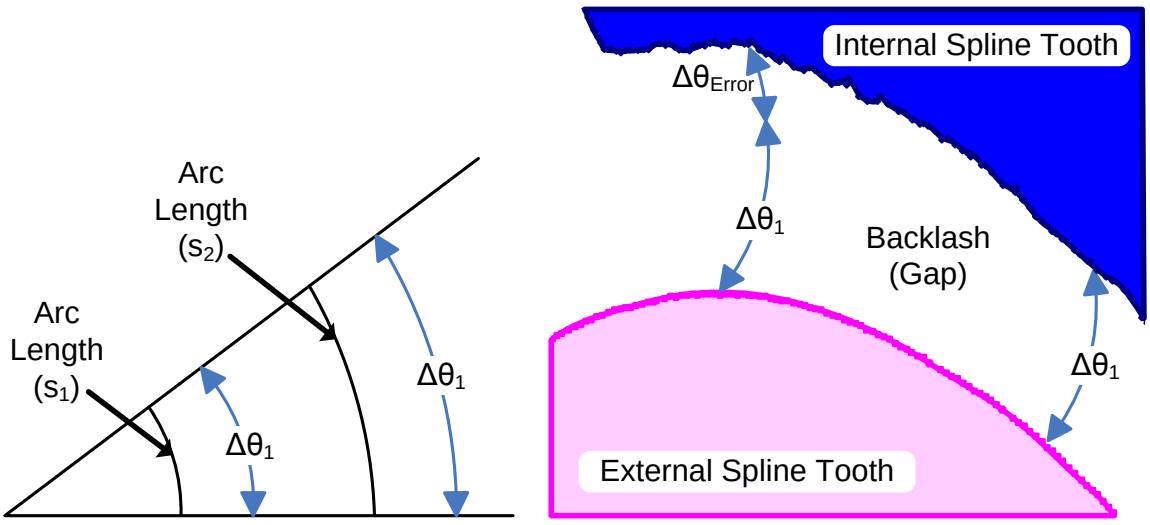

Figure 5-3 Arc length with constant theta (left) and exaggerated tooth pair contact (right)

Recall, with two perfectly mating involute flanks, the arc length travel between two contacting points increases with radial distance; however, the change in angle ($\Delta\theta$) required to engage the flanks is constant, as shown on the left of Figure 5-3.

It can be seen that the $\Delta\theta$ at each point is not constant as they should be for two perfect mating involute profiles. Therefore, the region along the flank with the smallest $\Delta\theta$ will be the place where contact occurs first.

As shown in the right of Figure 5-3, the initial tooth contact will first occur to the right, which is near the tip of the external tooth and at the root of the internal tooth. As the external tooth deflects, the clearance diminishes over the entire gap and the contact region increases towards the root of the external tooth.

5.3 Calculating Angular Rotation to Engage Teeth

In order to determine the necessary angular rotation to engage each tooth pair, the internal and external data sets were first filtered to reduce the number of calculations that would be required with such large data sets. Engagement will only occur on the involute profile region and only one side of each tooth, the left flank, was considered; therefore, a filter was devised to eliminate all data sets that did not meet these criteria. The filtered internal and external spline data sets were reduced from 26,000 each to approximately 8,500 each. The steps used to calculate the angular rotation between tooth pairs are described as follows:

1. All data was converted from Cartesian (X, Y) to polar coordinates (R, θ).
2. A R_e value on the 1st flank of the external spline was selected.
3. The closest R_i value on the mating flank of the internal spline was located.
4. The θ_i value corresponding to the newly found R_i value was returned
5. This θ_i value was then differenced from θ_e to give $\Delta\theta$.
6. $\Delta\theta$ is the angular rotation required before the two points make contact.

The process described above was automated, and an angular rotation ($\Delta\theta$) was calculated at each point along the profile of the first flank of the external spline. The average of the five smallest $\Delta\theta$ values was used in order to estimate the contact region. The $\Delta\theta_{ave}$ values were then calculated for the remaining 64 tooth pairs. The results are shown in Figure 5-4 which is a plot of the tooth-to-tooth clearance of the 65 tooth pairs in the first assembled configuration.

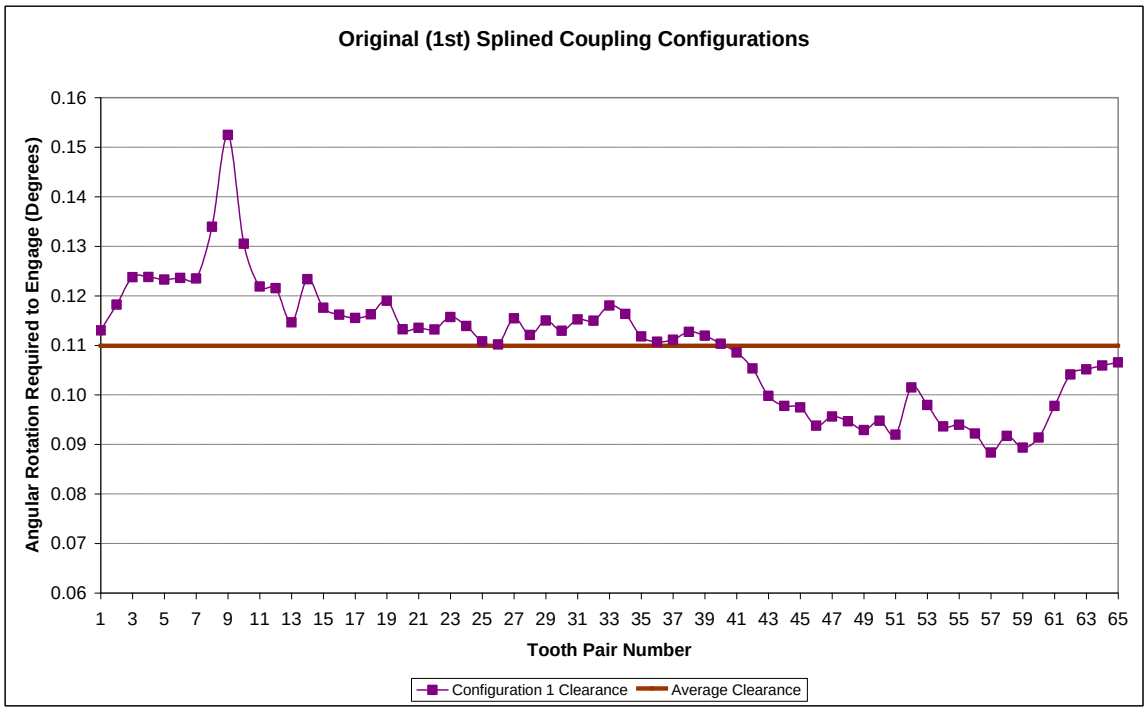

Figure 5-4 Tooth-to-tooth clearance in original (1st) configuration

From this initial analysis of tooth engagement, as shown in Figure 5-4, a trend can readily be seen. The lowest points show in Figure 5-4 represent the tooth pairs that will engage first. Therefore, tooth pair number 57 will be the first to engage, followed by 59, 60, 58, 51, etc, while the last tooth pair, number 9 and many preceding it like 10, 8, 4, etc, will never engage because the maximum load has been reached and the other tooth pairs already carry the full load. Table 5-1 summarizes the analysis shown in Figure 5-4,

Table 5-1 Summary statistics for original (1st) configuration

Rotation required for first tooth to engage (backlash)	0.088°
Deflection of first tooth when last tooth engages	0.064°
Average deflection of all teeth	0.11°

The results shown in Figure 5-4 are specific to the original or first configuration of 65. The spline coupling can be assembled in 65 different configurations and each configuration will result in a different tooth engagement profile. In order to test each of the 65 configurations the external gear remained fixed and the internal gear was rotated one tooth pair and the clearances between tooth pairs was recalculated. This analysis was performed on each of the 65 different configurations.

Of the 65 possible configurations, Figure 5-5 shows two configurations of interest: configuration 16 and configuration 42. These two configurations were selected because configuration 16 displays the least amount of variance, while configuration 42 exhibits the largest variance.

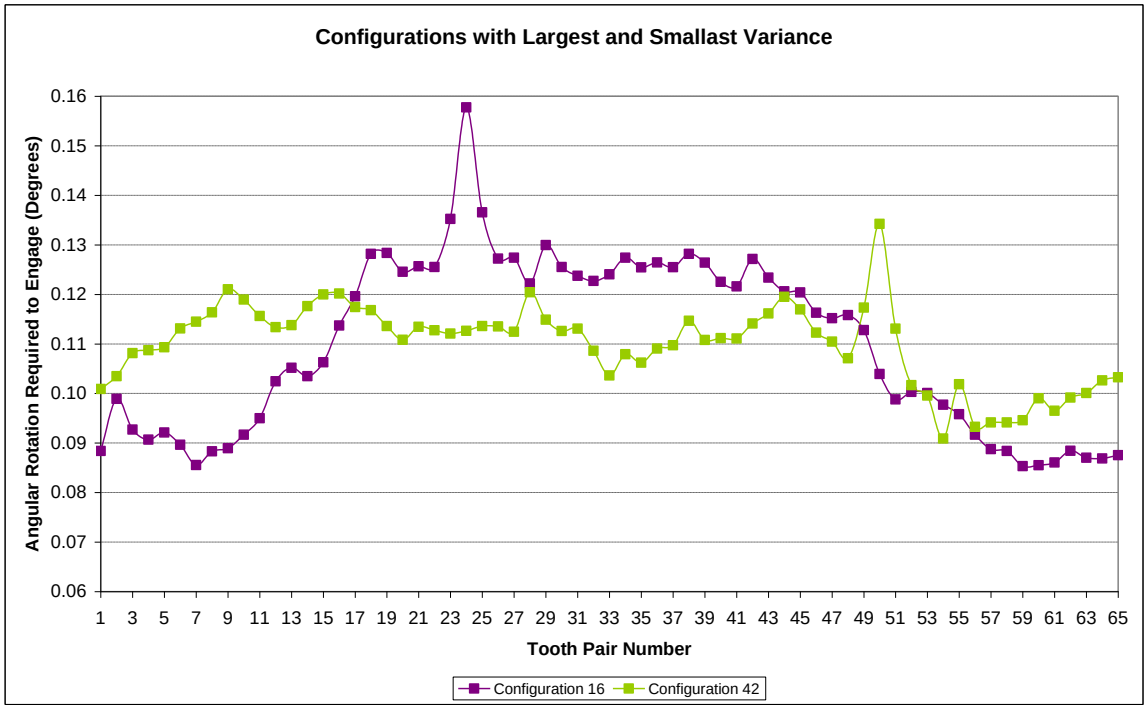

Figure 5-5 Angular rotation required to engage teeth for configuration 16 and 42

It can be seen from Figure 5-5 that while the assembly is in the 16th configuration, tooth pair 59, 60, and 7 will engage first and tooth pair 50 will be the last to engage. Table 5-2 shows the summary statistics of tooth engagement for these two configurations.

Table 5-2 Summary of tooth engagement for the 16th and 42nd configurations

	Conf. 16	Conf. 42
Rotation required for first tooth to engage (backlash)	0.085°	0.091°
Deflection of first tooth when last tooth engages	0.072°	0.043°
Average deflection of all teeth	0.025°	0.019°

Figure 5-5 shows the data plotted by location, whereas Figure 5-6 shows the same data sorted by engagement, where the results of these two configurations are sorted from first to last pair to engage.

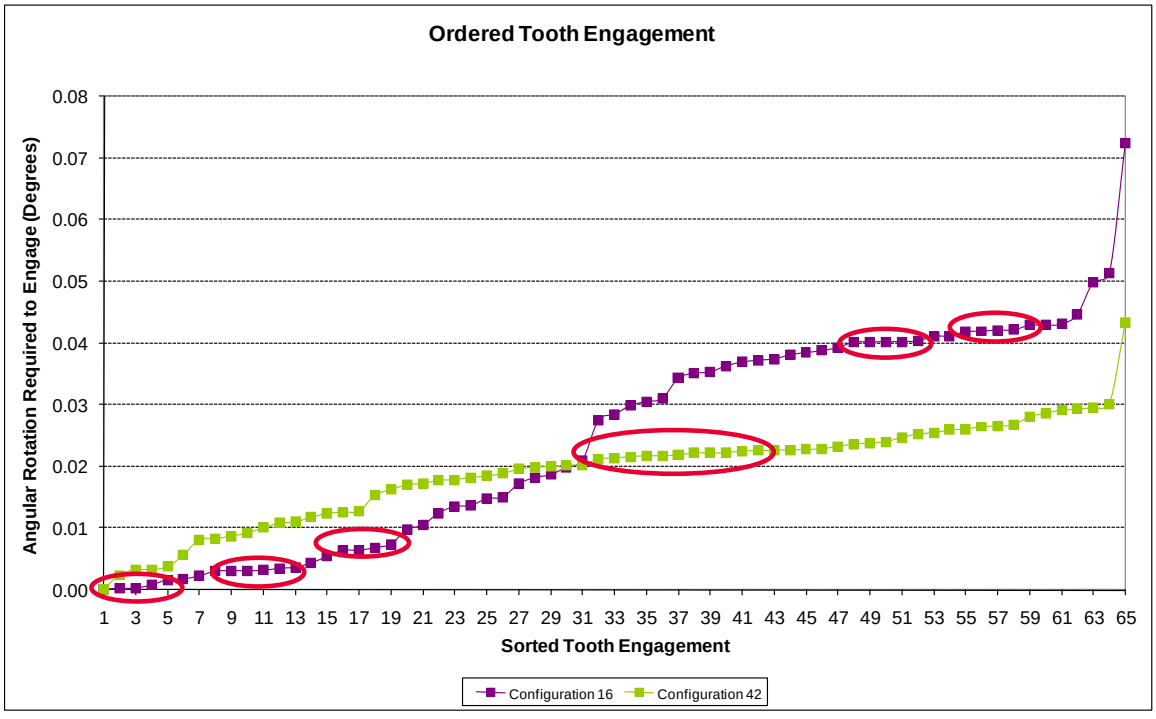

Figure 5-6 Ordered tooth engagement for the 16th and 42nd configurations

After reviewing the preceding figure and table it appears that configuration 42 would result in better load carrying capacity because it has less variance and, as shown in Table 5-2, the deflection of the first tooth when the last tooth engages is smaller. However, Figure 5-6 reveals another important consideration: that of quasi-simultaneous tooth engagement.

The first tooth pairs to engage carry more load than the following tooth pairs; therefore, the initial engagement pattern is of considerable importance. Figure 5-7 shows a closer look at the first eleven tooth pairs and reveals some quasi-simultaneous tooth engagement in configuration 16.

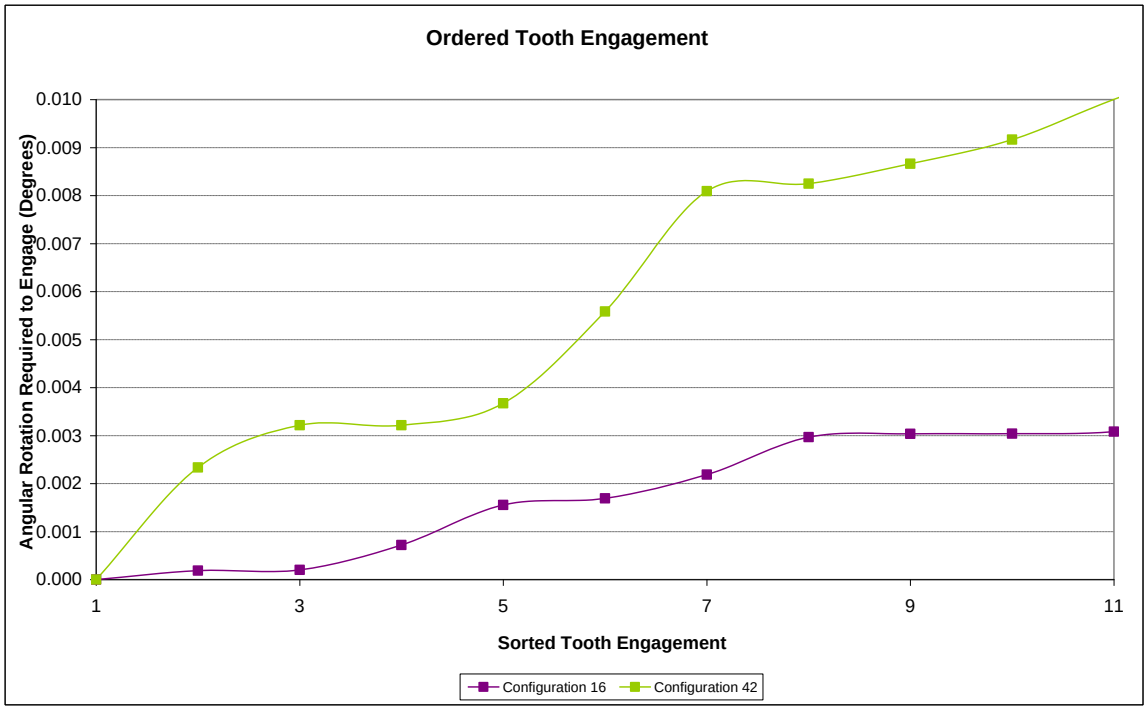

Figure 5-7 First 11 tooth pairs to engage

It can be seen in Figure 5-7 that a mere deflection of 0.001° is required for the first four tooth pairs to engage. This quasi-simultaneous tooth engagement means four tooth pairs will have to deflect for a fifth to engage, instead of one; therefore, the resulting torque deflection curve better approaches the ideal curve as was explained in Chapter 1 and shown in Figure 1-7. On the other hand, configuration 42, which has less overall variance, has greater variance in the initial 11 tooth pairs. To further this point, it is shown that when the seventh tooth pair engages in configuration 16, only one tooth pair has engaged in configuration 42.

5.4 Conclusions

There is a wave-like pattern in tooth engagement profiles. Of the 65 different assembly configurations there is one with the least overall variation and one with the most overall variation (16 and 42 respectively). Furthermore, the configurations with the best tooth engagement profile are those with the least variation between the first tooth pairs, resulting in early quasi-simultaneous tooth engagement.

Chapter 6 Calculation of Tooth Deflection Constant K

The previous chapter provides an in depth analysis of how two imperfect splines make contact with each other. This chapter provides an analytical model of two mating teeth to determine the stiffness of the pair. This model, when coupled with the tooth contact variation, provides the information necessary to analytically recreate a torque-deflection curve for the spline coupling, and then compare the analytical results with the experimental results.

6.1 Overview

In order to recreate a torque-deflection curve for the measured data, the tooth clearances and tooth stiffness values must be known. The tooth pair clearances were calculated earlier in Chapter 5 and were ordered from smallest to largest angular clearance, as shown previously in Figure 5-6. To complete the model, all that is necessary is to calculate the tooth stiffness values. Each tooth on the splines was treated as a spring of stiffness K. As two teeth engage, both teeth deflect; therefore, an equivalent tooth pair stiffness can be found by adding the internal and external stiffness values together as reciprocals, the same way one would add two springs in series. Once the first pair of teeth has deflected enough for the second pair to engage, then the first equivalent tooth pair stiffness can be added to the second in parallel.

6.2 Simplified Tooth Model

In a previous study, a simplified tooth model was developed and verified by finite element modeling in order to estimate the internal and external tooth stiffness values (K_i and K_e, respectively). The simplified tooth model approximates the involute tooth as a tapered beam as shown in Figure 6-1 [7].

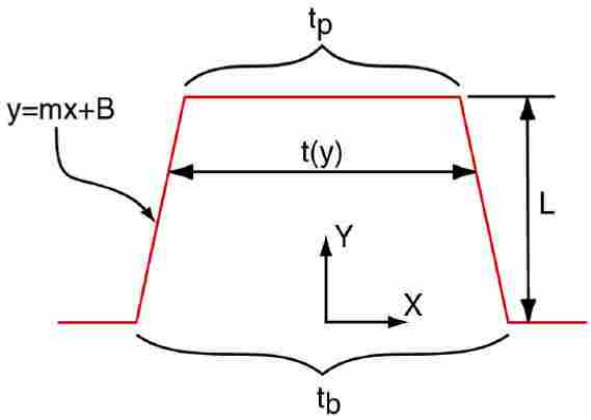

Figure 6-1 Simplified tooth model used in calculating tooth stiffness

The deflection of the simplified tapered beams can be calculated by adding the deflection due to bending and the deflection due to shear using Equation (6-1) where B, m and L are chosen for external or internal spline teeth [7]

$$\delta_{total} = \delta_{bending} + \delta_{shear} = \frac{12F_t m^3}{8El}\int_0^L \frac{y^2}{(B-y)^3}dy + \frac{F_t m}{k_s Gl}\int_0^L \frac{}{B} \tag{6-1}$$

and where G is the modulus of rigidity and is calculated using Equation (6-2).

$$G = \frac{E}{2(1+\mu)} \tag{6-2}$$

Equations (6-3) and (6-4) convert from torque to force and vice versa.

$$K = \frac{F_t}{\delta_{total}} \tag{6-3}$$

$$T = K\theta = F_t R_c \tag{6-4}$$

The geometric parameters of this simplified tooth model of the internal and external teeth were estimated by importing the measurement data for a single tooth as a CAD model, then drawing a tapered beam to approximate the involute tooth as shown in Figure 6-2. Previous work didn't use measurement data, but rather fit a tapered beam to a theoretical tooth profile of a spline coupling with 100 teeth.

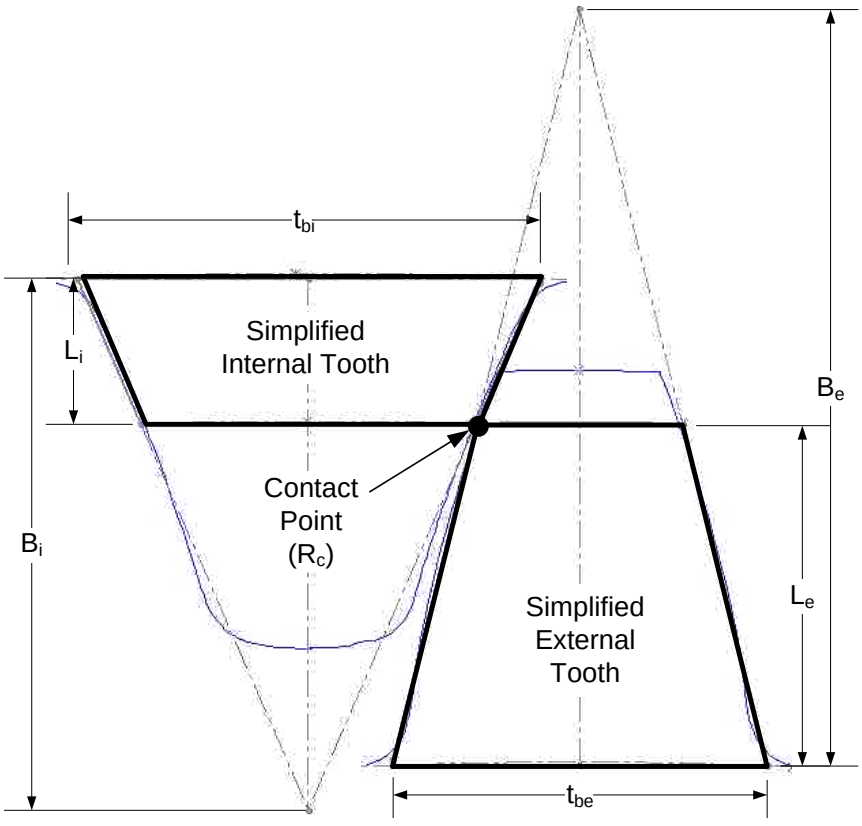

Figure 6-2 Estimating parameters for simplified tooth model

Each tooth on the external spline is slightly different due to process variations; therefore, a unique stiffness value could be calculated for each tooth. However, for this analysis, only one stiffness constant was calculated for each spline. This simplification is justified for two reasons: first, the variation between tooth stiffness values will be very small, and second, the error associated with the simplified tooth model is larger than any error associated with assuming all teeth on a single spline have the same stiffness constant. Therefore, it was only necessary to calculate the tooth stiffness of one tooth on each spline and then use those values in determining the torque deflection curve for the spline coupling. The parameters that describe the simplified tooth profiles are summarize in Table 6-1 along with the material properties of alloy steel. Radii values are measured from the center of the spline while other parameters are measured as shown in Figure 6-2.

Table 6-1 Summary of values used to calculate tooth stiffness values

Description	Var.	Int. (i)	Ext. (e)	Units
Radius at the pitch circle	R_p	103.183	103.183	mm
Radius at root of spline	R_r	109.160	100.054	mm
Radial tooth pair contact point	R_c	106.394	106.394	mm
Pressure angle at contact pt. R_c	Φ	23.48	13.9	deg.
Distance from root to contact R_c	L	2.766	6.340	mm
Y intercept of tooth model	B	9.936	14.142	mm
Half the tooth thickness at base	$t_b/2$	4.316	3.495	mm
Slope of line on tooth model	m	2.302	4.046	none
Axial length of the spline tooth	l	3.18	9.54	mm
Poisson's ratio	μ	0.28	0.28	none
Modulus of elasticity	E	30	30	Mpsi
Modulus of rigidity	G	11.72	11.72	Mpsi
Shear constant (rectangle)	k_s	5/3	5/3	none

For splines, both profiles are generated from a common base circle, with the same tooth spacing. Therefore, when two perfect involute profiles engage, one internal and the

other external, the two surfaces are in full contact. However, due to variation, the splines do not experience full surface-to-surface contact. Furthermore, as the load is applied, deflections cause the radius of the external tooth profile to decrease, while the internal radius increases, creating additional mismatch. Hence, the contact between teeth is more likely a small region, centered on a point. Note that contact occurs at a radius Rc, which is greater than the pitch radius Rp.

Figure 6-3 shows the analysis of the contact zone on the first pair of teeth. The x-axis shows the angular rotation required before the teeth will engage and the y-axis shows the radial location where that engagement occurs. If the two profiles were perfectly involute, the graph would show the same angular clearance independent of the radial location (a perfectly vertical line). However, due to variation, the actual profile deviates from the perfectly involute profile, as shown in Figure 6-3.

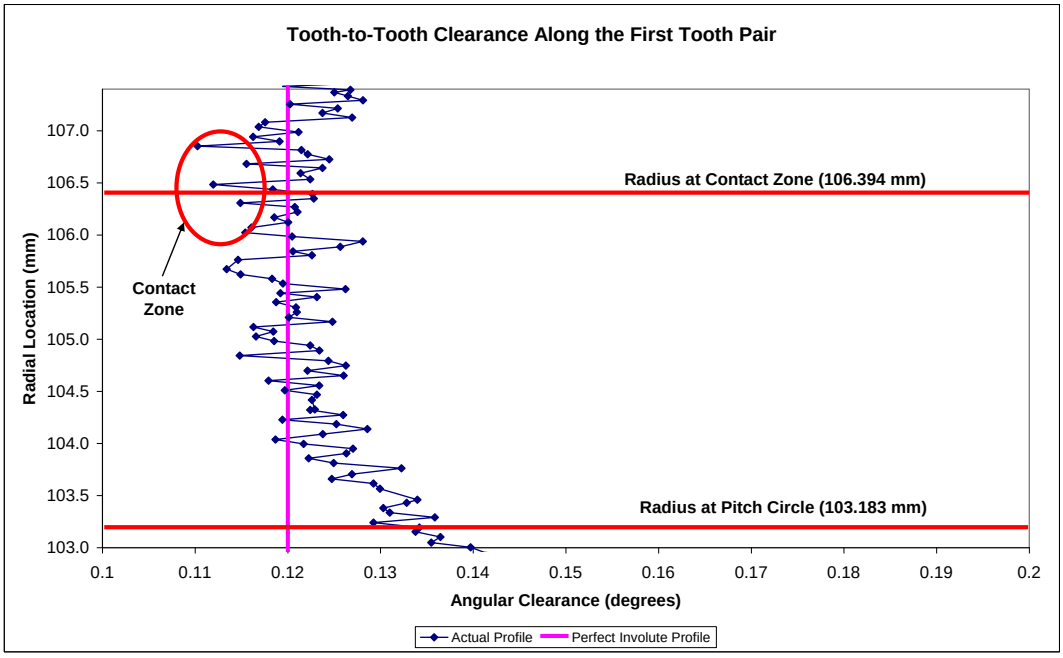

Figure 6-3 Clearance profile of the first tooth pair to engage

The simplified tooth model used by DeCaires takes into account that tooth-to-tooth contact will begin at a point in order to calculate tooth deflections. The contact point was assumed to occur at the pitch radius, Rp. However, the measured profile data in Figure 6-3 illustrates that the assumed contact point of Rp on the first tooth pair is inaccurate and that the actual contact point occurs farther out than the pitch circle (about 106.4mm), where the clearance is minimum. Therefore, an analysis on all the tooth pairs was performed to determine the unique contact point for each pair. The average contact radius was found to be Rc = 106.394 mm. The results are plotted in Figure 6-4.

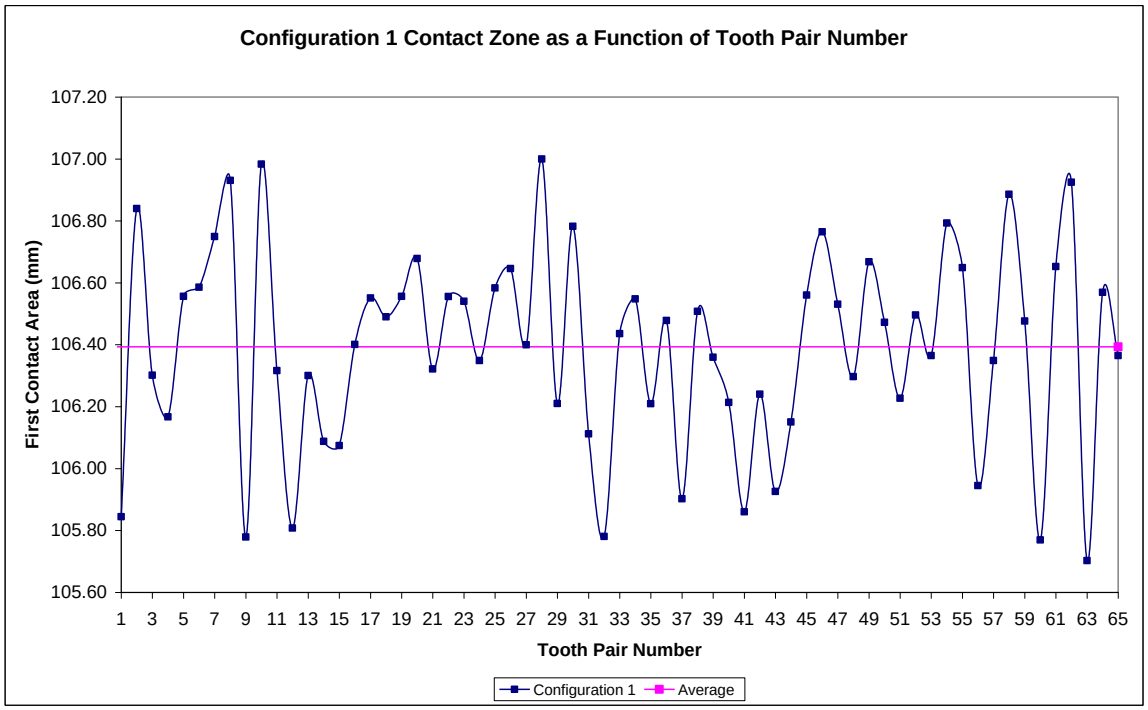

Figure 6-4 Radial location of first contact between mating tooth pairs

Figure 6-4 shows that on average the teeth make first contact a radial distance of 106.394mm instead of at the pitch circle, where Rp=103.183mm. This difference is

important in that it changes the stiffness values of the internal and external teeth and reduces the overall stiffness of the pair. To illustrate this, consider the following: if the contact is made at the pitch circle, then we would expect Ki>Ke because the cross-sectional area of the internal tooth is greater than the external tooth. If Ki were to equal Ke, then, when the two are added in series Keq= 0.5Ke=0.5Ki. However, since Ki>Ke then Keq is reduced below the maximum of 0.5Ki. Therefore, Keq is maximized as the two individual stiffness values become equal. However, tooth contact occurs at Rc instead of Rp, therefore Ke is reduced and Ki is increased, resulting in a lower the overall Keq value.

Using the aforementioned equations and the values from Table 6-1 (all values were converted to their base units prior to performing the calculations), the following results were obtained, as summarized in Table 6-2.

Table 6-2 Summary of tooth stiffness calculations

Description	Var.	Internal (i)	External (e)	Units
Torque	T	1.00	1.00	Nm
Force total	F_{total}	9.40	9.40	N
Force (tangential) applied to tooth	F_t	9.10	9.10	N
Deflection from bending stress	$\delta_{bending}$	3.77E-09	5.15E-08	m
Deflection from shear stress	δ_{shear}	1.60E-08	1.70E-08	m
Total tooth deflection (tangential)	δL_{total}	1.97E-08	6.85E-08	m
Total tooth deflection (angular)	$\delta\theta_{total}$	1.85E-07	6.44E-07	rad
Spring constant of a single tooth	K_1	5.39E+06	1.55E+06	Nm/rad

Detailed step-by-step calculations for the results summarized in Table 6-2 are found in Appendix C. With the individual spring constants of internal and external spline

teeth shown in Table 6-2, an equivalent spring constant for the pair was determined by adding K_i and K_e together in series using Equation (6-5).

$$Keq_1 = \left(\frac{1}{K_i} + \frac{1}{K_e} \right)^{-1} \tag{6-5}$$

The resultant equivalent spring constant for a single tooth pair was determined to be $Keq_1 = 1.22 \times 10^6$ Nm/rad. As additional tooth pairs engage, the equivalent spring constants for each tooth pair can be added together linearly, like two springs in parallel. Therefore, any number (n) of tooth pairs engaged can be calculated using Equation (6-6).

$$K_n = nK_1 \tag{6-6}$$

An analytical torque deflection curve can be created by summing the stiffness of the tooth pairs as they engage. This produces a torque-deflection curve whose slope increases incrementally. Because the tooth pairs do not engage simultaneously, it is necessary to determine the clearance between each tooth pair in order to determine how much deflection will be required before the next tooth pair engages. From the analysis performed in previous chapters, the angular rotation required for each tooth pair to engage was determined and the results were shown in Figure 4-3. Using the ordered deflection data, a torque displacement curve was created, as shown in Figure 6-5.

As was shown in Figure 5-7 the first tooth engagement occurs at 0.085 degrees; therefore, this is the backlash or clearance held in common between all teeth and can be removed so that the engagement profiles shown in Figure 6-5 all start at zero. This removal of backlash allows the experimental results to be compared to the analytical data which were adjusted to begin at zero.

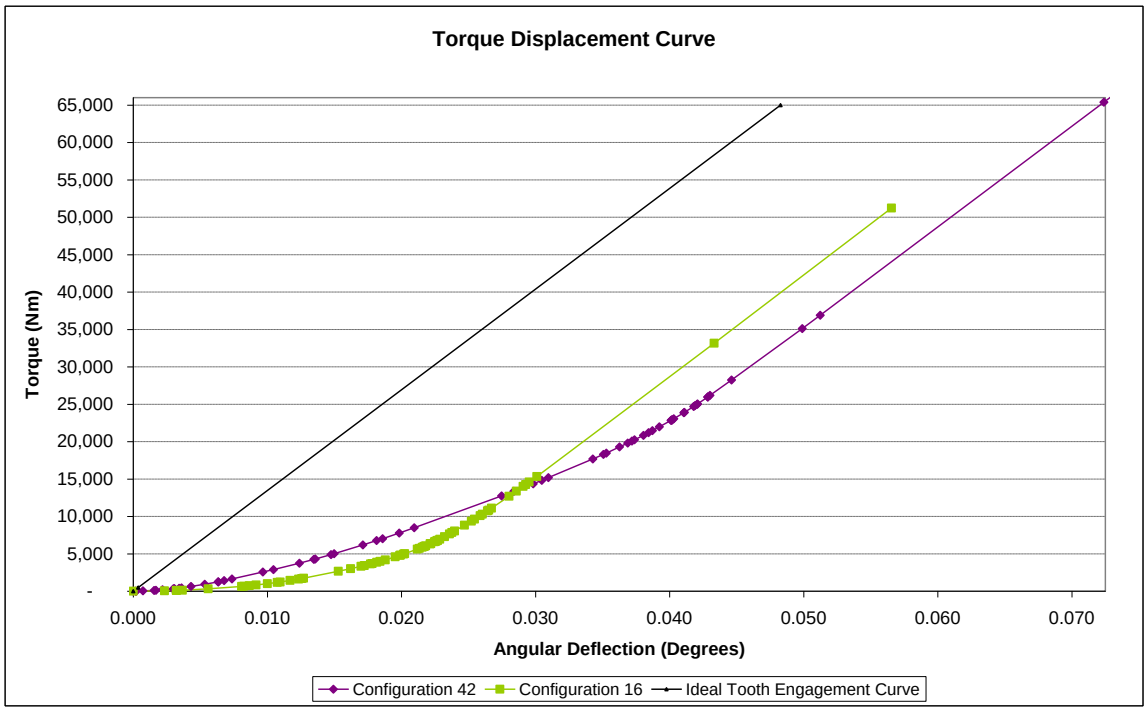

Figure 6-5 Analytically determined torque displacement curve

The analytical results of the measurement data clearly confirm a sequential tooth engagement model; however, a few interesting things can be noted from Figure 6-5. The ideal tooth engagement curve represents the best possible tooth engagement of all 65 teeth engaging simultaneously. Configuration 42, which is the configuration with the most overall variance, will require about 65,000 Nm of torque in order for the 65th tooth pair to engage, while configuration 16 will require about 51,000 Nm (Note: tooth failure will occur before these loads can be reached). Because configuration 42 has early quasi-simultaneous tooth engagement it better approaches the ideal curve than configuration 16. It can also be seen in Figure 6-5 that the terminal slopes of the three different analytical profiles is the same as the slope of the ideal tooth engagement curve, which should be expected.

Next, these results were compared to the force-deflection curves obtained experimentally and the x and y scales were adjusted to display the analytical results on the same scale as the experimental results. Significant discrepancies are apparent between the analytical and experimental results as shown in Figure 6-6.

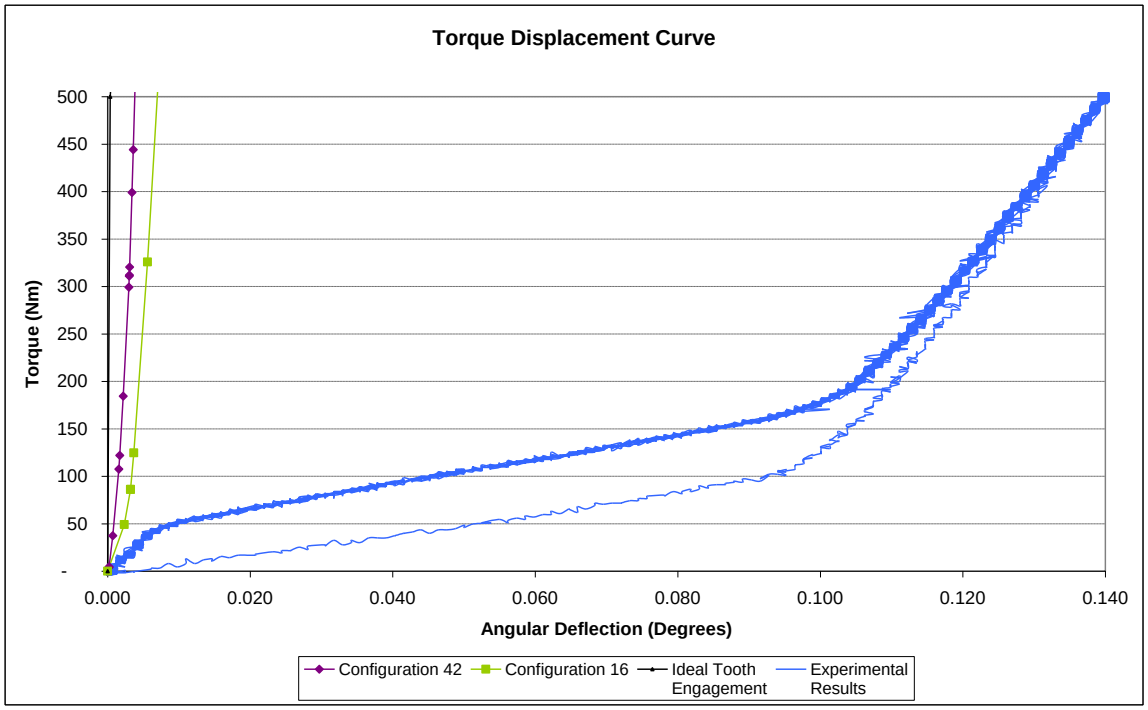

Figure 6-6 Comparison of analytical and experimental force deflection curves

The results shown in Figure 6-6 show that the slope of the first line segment on any of the analytical results is much greater than any slope on the experimental curve. This means the experimental stiffness was always significantly less than the analytical results. Due to this difference the experimental setup was reviewed in order to determine the source of lower stiffness that was measured.

6.3 Review of Experimental Setup

In order for the experimental stiffness to be so much less than that predicted by the analytical results, there must be other components in the setup with lower stiffness that, when added in series with the equivalent tooth pair stiffness, significantly reduce the overall stiffness of the system. Figure 6-7 shows a photo of the experimental setup that was used along with labels detailing the different components in the setup.

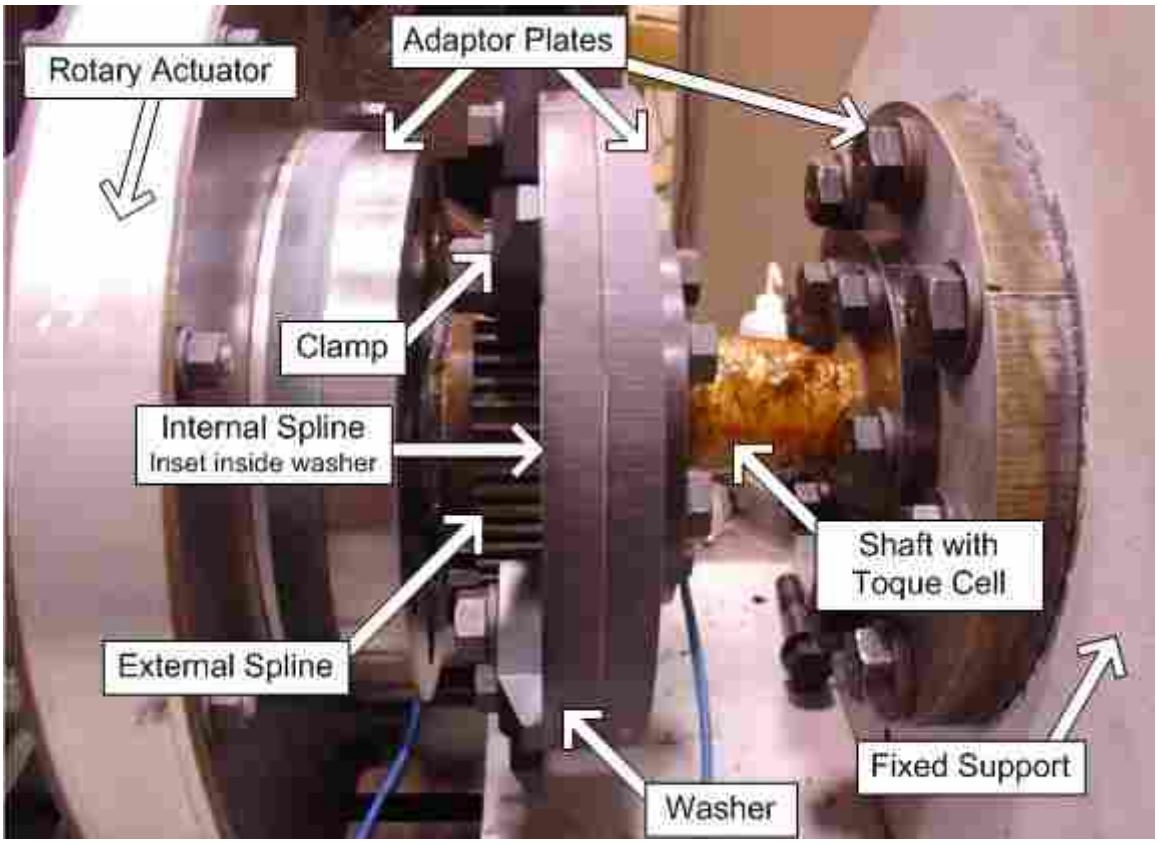

Figure 6-7 Industrial partner experimental test

The only way for torque to be transmitted to the torque cell on the right is for the external teeth to transmit torque to the internal teeth. However, due to the setup, torque

transmission is not that simple. The following is a more detailed description of torque transfer in the experimental setup shown in Figure 6-7. As the actuator (on the left) rotates the external spline shaft, the teeth on the external spline engage with the teeth on the internal spline. The internal spline is held in place by friction from the lugs and the washer. This friction is created by tightening the bolts that go through the lug and washer and then threaded into the adaptor plate. The adapter plate then transfers the torque to another adjoining adaptor plate (fastened with six bolts) and then to the shaft whereon the torque cell is mounted. This setup brings into question three potential sources of unwanted deflection: 1) the shaft whereon the torque cell is mounted, 2) frictional sliding as the bolts adjust within the lugs and adaptor plates and 3) the deflection of the bolts in the setup

6.4 Analytical Model for Shaft Deflection

Adding the shaft stiffness into the analytical model changes the torque deflection curve by reducing the overall stiffness of the model and thereby more closely resembles the experimental results as shown in Figure 6-8. It is also shown in Figure 6-8 that when the torque load cell shaft is included in the stiffness model, sequential tooth engagement is less visible because the incremental slope changes are less pronounced due to the flexible shaft dominating the deflection results. If the model is changed and the shaft diameter is doubled, then the tooth engagement becomes more pronounced. Table 6-3 summarizes the values and results used in calculating the shaft stiffness.

Table 6-3 Values and results of torque load cell shaft stiffness calculation

Description	Var.	Shaft	Units
Diameter of shaft	Ds	0.053	m
Length of shaft	Ls	0.090	m
Modulus of rigidity	G	8.1E+10	Pa
Moment of inertia of a circle	J	7.68E-07	m^4
Spring constant (angular)	K_s	6.90E+05	Nm/rad
Radial tooth pair contact point	Rc	0.106394	m
Torque	T	1.00	Nm
Shaft deflection (angular)	δ_s	1.45E-06	rad

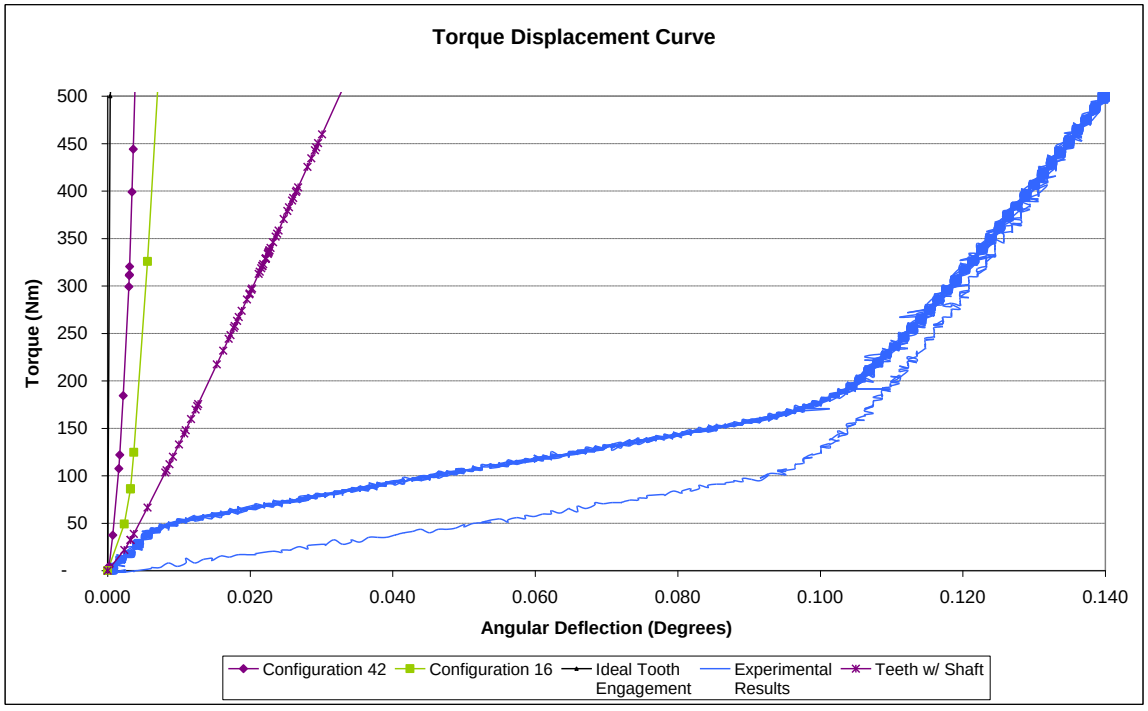

Figure 6-8 Torque deflection curve accounting for shaft stiffness

Figure 6-8 shows the resulting torque deflection profile when the torque load cell stiffness is accounted for. The initial and final slopes better approximate the experimental results.

To illustrate the significance of less stiff members in series with the splines in the experimental setup, three different shaft sizes were used in the calculations and the

resulting tooth engagement profiles are shown in Figure 6-9 (Note, the vertical scale differs from Figure 6-8).

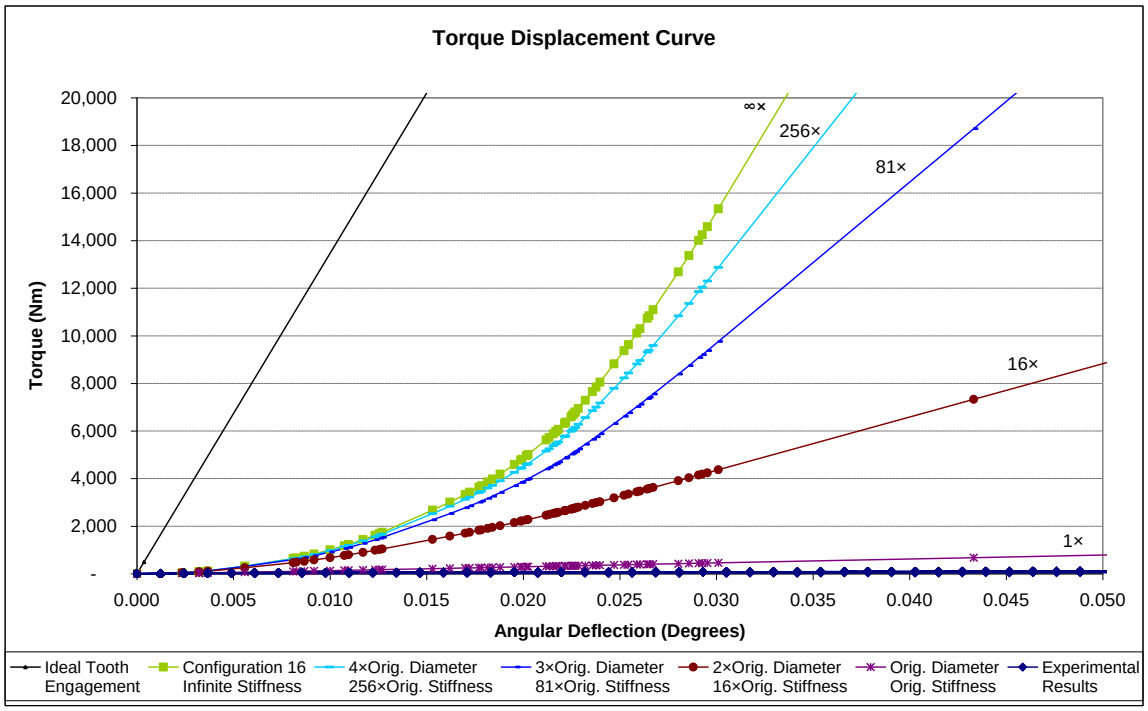

Figure 6-9 Comparison of larger diameter shafts used in analytical calculations

The diameter (D) of the supporting shaft is critical because its value increases by the 4^{th} power in calculating the moment of inertia (J) that is used in calculating the stiffness constant (K) of the shaft using Equations (6-7) and (6-8), where G represents the modulus of rigidity and L represents the length of the shaft.

$$J = \frac{\pi \cdot D^4}{32} \tag{6-7}$$

$$K = \frac{G \cdot J}{L} \tag{6-8}$$

It has been shown that by including the torque load cell in the model, the analytical results begin to approximate the steep slope of the experimental results as seen in Figure 6-8. Therefore, by taking into account other members of the assembly, like the external spline shaft, the analytical results will more closely match the experimental results.

The shallow slope, shown in the experimental results, may be the result of slippage in a friction joint, like the bolts and clamps securing the members in the assembly. Figure 6-10, shows a possible schematic that could result in a torque deflection curve like that shown in the experimental results. The schematic shows two springs K1 and K2 connected in parallel with a slip joint. As a load is applied both K1 and K2 carry the load in parallel until the split joint begins to slip. During slipping, K2 carries the load until the slip joint stops and again K1 and K2 carry the load. As the setup is unloaded a different path is followed due to reverse slip.

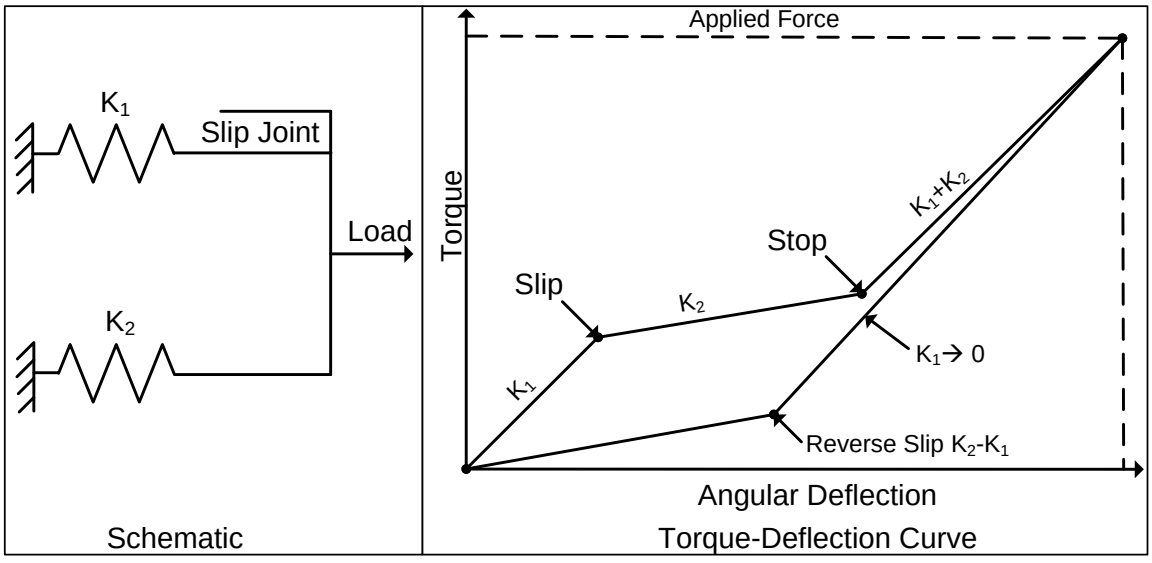

Figure 6-10 Schematic that would result in the experimental torque-deflection curve

This schematic represents one possible way of recreating the unusual torque-deflection curve that was obtained experimentally. It is not important in this study to understand exactly how the setup fixture bolts, friction and shaft contribute to the measurement data. The important thing is to illustrate that the results are more likely a function of the setup than the spline coupling. To validate this, the same setup could be repeated, but external spline could be completely welded to the supporting ring and then re-tested to see if the results are similar.

As an additional note, due to the significant noise that was measured from the experimental setup, the 3 curves that were obtained experimentally cannot be matched up with any of the 65 analytically calculated configurations.

6.5 Conclusions and Recommendations

The initial experiment has revealed some invaluable results, which have aided in the understanding of tooth deflection and the resulting torque-deflection curves. The applied torque-rotation plots did exhibit a nonlinear stiffness, which increased incrementally, indicating sequential tooth engagement. However, attempts to re-create the plots from raw spline profile measurements and analytically-derived tooth stiffness models failed. The stiffness magnitudes did not match and the experimental plots exhibited a hysteresis loop, not predicted analytically.

It has been shown that the stiffness of the components of the experimental setup play a significant role in the experimental results. Specifically, the shaft and fixture deflections in the experimental setup contributed so much to the results that the tooth engagement stiffness could not be measured independently. Therefore, it is

recommended that an experimental setup be used such that the teeth on the splines are the most flexible components of the setup. A stiffer design requires that the bolts and shaft be stiffened or that a new design be used in order to completely bypass the need for these members. For example, a new design might entail welding the internal spline to a fixed support in a manner similar to the external spline. Perhaps a rotary actuator that is capable of outputting both torque and angular rotation data would be needed because a strain gage applied to a larger diameter member in series would no longer provide the necessary resolution. The key in the setup is to minimize the deflection that can occur at welds, bolted connections, and at smaller members, while maintaining high resolution of the torque deflection data output. One recommendation is to put the torque sensor in series with the actuator and mount the internal splines plate directly to the rigid frame. Then, if the rotation could be measured directly on the external spline shaft, intermediate deflections could be eliminated.

Chapter 7 Spline Manufacturing

In order to understand variation associated with splines and tooth engagement, the source of the variation must be better understood: manufacturing. Previous chapters showed non-random errors associated with the individual splines and the assembly. Repetitive error patterns may originate from manufacturing tools, setup, and other associated processes. There are many processes and tools used in gear manufacturing (see diagram in Appendix B); however, the scope of this work will concentrate on a manufacturing process known as hobbing, with brief consideration given to broaching. Though the exact manufacturing method of the tested splines is unknown, after consulting with a geometrician and the industrial partner, hobbing and broaching seemed like the most likely processes used in manufacturing the external and internal splines, respectively.

7.1 Hobbing Overview

A hob is a hardened cylindrical cutter for machining gear teeth on a metal gear blank [5]. The hob closely resembles a worm gear with one or more threads that follow a helical path along the length of a cylinder. In order to create the cutting faces on a hob, a series of equally spaced flutes (gashes) are cut along the axial plane. Figure 7-1 and Figure 7-2 show a typical hob from a plane of rotation view and an axial view,

respectively. Typical terminology used to describe hobs can be found in the ANSI/AMGA Standard 1102-A03 (see Appendix E).

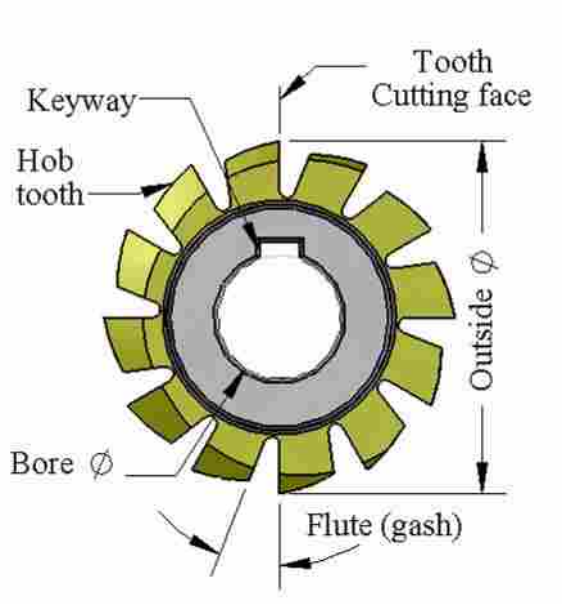

Figure 7-1 Plane of rotation view of hob

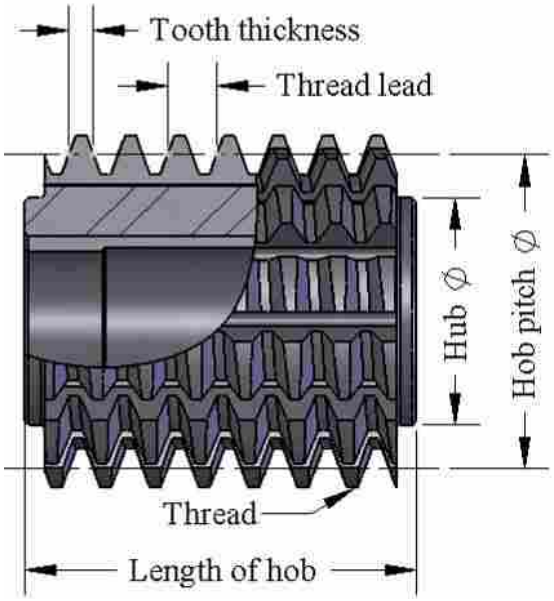

Figure 7-2 Axial plane view of hob

The hobbing process is carried out on special machines, where a hob is positioned by the spline blank and fed axially as it rotates, creating grooves between the splines, as shown in Figure 7-3. The spline blank and hob are separately rotated in a synchronized manner, at a calculated ratio to generate the appropriate number of teeth on the spline blank. The hob is slowly fed parallel to the shaft axis, machining straight grooves as it rotates, transversing the blank, until all of the teeth on spline are generated to the required length. The thread angle of the hob and rotation of the shaft are set such that all of the spline teeth are generated in one pass of the cutter (for video of hobbing see video 5.48 by Cleghorn [3]).

As the hob rotates, the cutting pattern is repeated again and again. Any error in the hob itself would then leave a repeating error pattern on the spline. This potential

source of error patterns is investigated in the sections which follow, to see if they might contribute to the clustered tooth engagement observed in the spline tests.

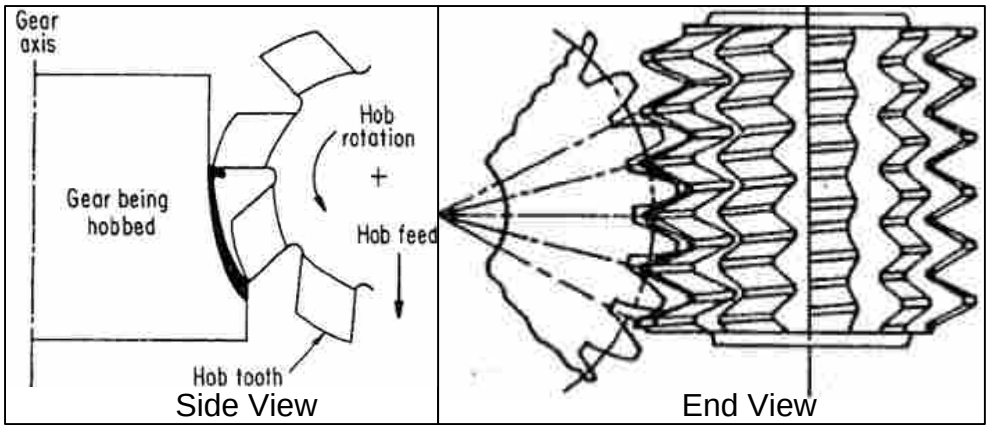

Figure 7-3 Illustration of hobbing process [5]

7.1.1 Hob Selection

Another area that has provided some insight into error patterning on spline couplings was found by studying hob designs and simulating the hobbing process. A 2D hobbing simulation program was created within Excel; the results suggest that error patterning may be more likely when a hob with multiple threads is used to cut a spline with an even number of teeth. Figure 7-4 shows some graphics obtained from the hobbing simulator used to create a 12 tooth gear with a single start hob. The results show a consistent pattern that every tooth will be cut the same. For example, if one of the hob cutting faces has been over-sharpened, then that error will be consistently mapped to every tooth on the generated spline independent of the number of teeth being generated.

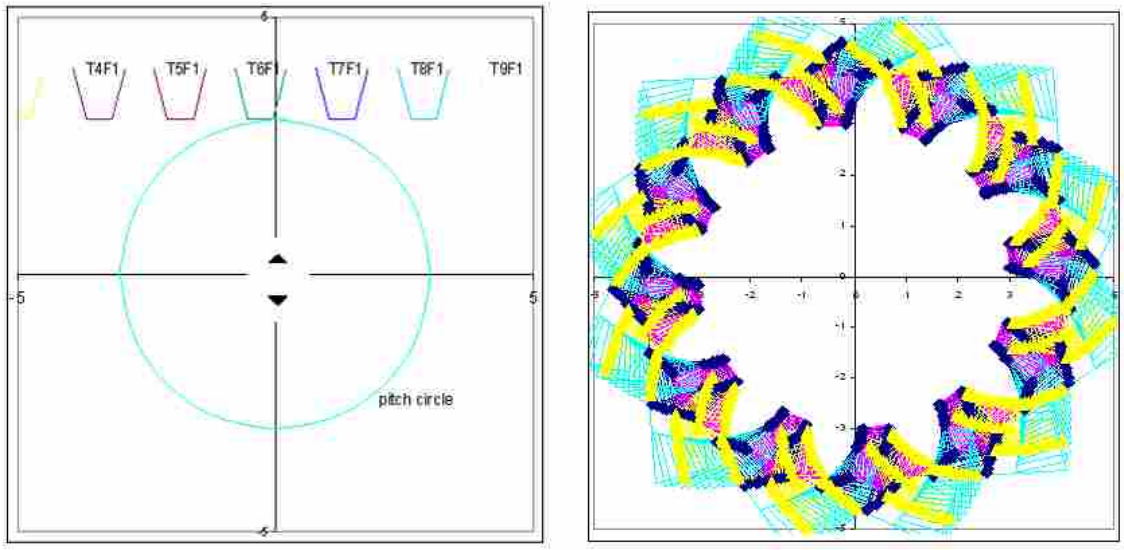

Figure 7-4 Rack and base circle (left) hobbing simulation with single start (right)

Figure 7-5 shows a close-up view of the involute tooth profile generated from a hob. The different colors are representative of individual cutting faces on the hob.

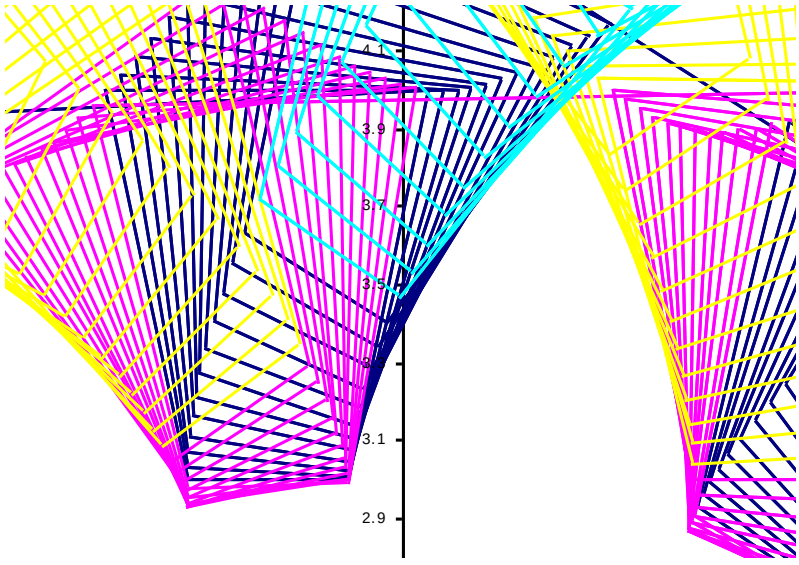

Figure 7-5 Close-up view of hobbing simulation

This consistent pattern demonstrated by a single start hob changes when multiple starts are considered. For example, a hob that has two starts functions differently. Like worm gears, a hob with two starts results in every other tooth being cut by a different thread as shown in Figure 7-6. This pattern shows that an external spline with an even number of teeth, if generated by a two-threaded hob (indicated in Figure 7-6 by the two colors) then the same thread is used to generate every other tooth and the other thread is used to generate the alternate teeth.

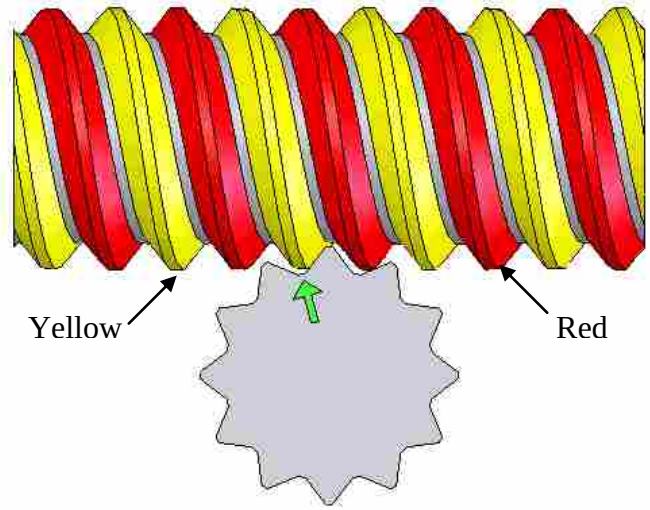

Figure 7-6 Worm gear with two starts and a spline with an even number of teeth (12)

Using Figure 7-6 as an example, this would mean the root generated by the yellow thread will never come in contact with the red thread. This non-uniform pattern would suggest that if the yellow thread were indexed wrong by a fraction of a degree, the result would be mapped to a specific set of teeth on the generated spline. This example illustrates the importance of hob selection in manufacturing gears. Special attention should be given to the number of starts on a hob and the number of teeth on the gear as

certain combinations like that shown in Figure 7-6 will not distribute hob errors uniformly across all teeth, resulting in periodic errors. To avoid this error the designer must calculate the ratio of the number of teeth to be cut and the number of starts on the hob. Table 7-1, used in the gear manufacturing industry, categorizes this ratio of number of teeth versus number of starts on the hob into three categories and describes the resulting errors.

Table 7-1 Hob selection criteria [17]

$\frac{Z_i}{Z} = \frac{\textbf{number of teeth on gear}}{\textbf{number of starts on hob}}$		
Prime	Common multiple	Even
Compensation total of circular pitch error **Best**	Compensation partial of circular pitch error **Okay**	Periodic error of circular pitch **Worst**

If the number of teeth on a gear is divided by the number of starts on the hob used to generate that gear there are three possible results: a non-terminating decimal, an integer, or a terminating decimal; these results correspond to the prime, common multiple, and even categories shown in Table 7-1. The following is a description of these three classifications where Z_i=the number of teeth on the gear and Z=the number of starts on the hob:

- **Prime:** if the division of the two numbers results in a non-terminating decimal, then the ratio is considered to be prime (i.e. 65/3=21.666…). Prime ratios occur when Z_i and Z have no factors in common but the number 1.

- **Common Multiple:** if the division of the two numbers results in an integer, then the ratio is classified as common multiple (i.e. 65/1=65). Common multiples only occur when Z_i is a multiple of Z.
- **Even:** if the division of the two numbers results in a terminating decimal, then the ratio is classified as even (i.e. 65/2=32.5). Even ratios occur when the greatest common factor of Z_i is not 1 or Z.

If a hob is selected to meet the prime ratio criteria, each thread will take part in generating each tooth, resulting in total compensation of circular pitch error. Prime ratios are the best choice in that it can compensate for any deviation errors due to hob mounting or any start indexing errors due to hob construction by equally distributing these errors among all teeth. When even ratios are used, as illustrated in Figure 7-6, there is no compensation for errors and instead, a periodic error pattern arises.

7.1.2 Faceted Teeth

The rotating action of a hob results in a many successive cuts. Though a hob may have straight sides, the accumulation of these cuts as shown in the left of Figure 7-7, results in a curved form on the gear teeth [10]. Figure 7-7 shows the resulting faceted involute profile that results from hobbing; however, in practice, the hob mesh of successive cuts is so fine that the facets become smooth.

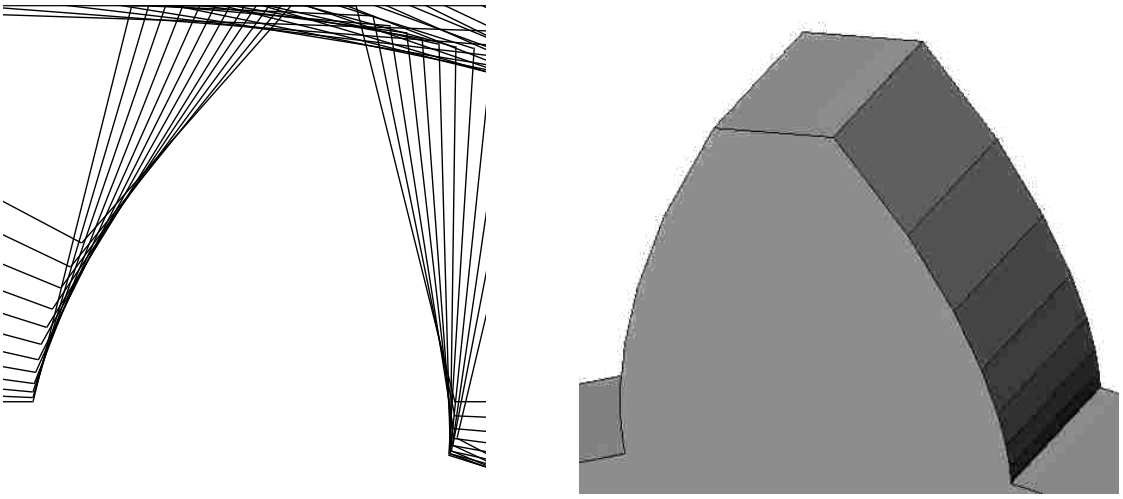

Figure 7-7 Demonstration of faceted flank

7.2 Broaching

Broaching is a machining operation which rapidly forms a contour in a workpiece by moving a cutter, called a broach, entirely past the workpiece (example shown in Figure 7-8). The broach has a long series of cutting teeth that gradually increase in height and are often used to cut internal gear teeth [6]. While broaching produces quite accurate gear teeth, the position of the finished gear teeth with respect to other features of the blank is sometimes difficult to hold [9]. However, the accuracy of a broaching operation can readily be compromised during setup resulting in significant eccentricity error. Furthermore, if a full-topping broach, one that cuts both the tips and roots, is not used, then the error profiles associated with the roots will differ from that of the tips.

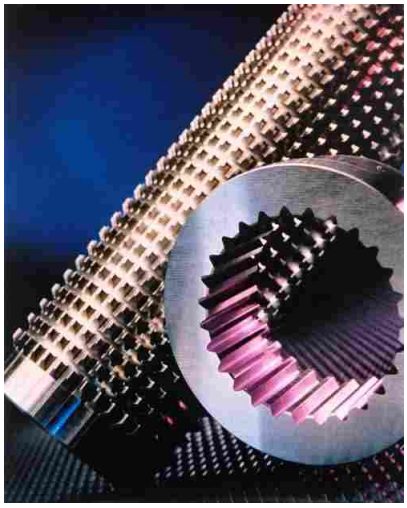

Figure 7-8: Example of a broach and resulting internal spline (broachmasters.com)

7.3 Conclusions

Error patterns were found to be created by several processes. CAD simulation demonstrated some. Other processes were found to successfully eliminate error patterns. For example, the 65 tooth spline studied herein is best hobbed using a hob with 3 starts in order to best compensate for pitch error, which is the composite error of the four error categories shown in Figure 2-5. The wave-like patterns from the analysis may be corrected with better hob selection and more accurate setups in order to avoid eccentricity error.

The misalignment in the wave-like patterns shown in roots and tips of the external spline could be the result of a non-topping generating process (see Appendix B for a breakdown of gear manufacturing methods). For example, a turning operation can be used to create a gear blank and that blank will have a center Ct. When the blank is placed in a hobbing machine the blank may not be mounted at exactly Ct, instead it may be

mounted at a slightly different center Ch. If a non-topping hob is used, then the hob will not remove any material at the tips of the external spline, which results in two different centers: Ct for the tips and Ch for the roots. Furthermore, if the ratio between gear teeth and hob starts is common or even, then another periodic error pattern can be transferred from the hob to the generated spline.

As error patterns became apparent in the analysis of the splines it became necessary to understand the source of these patterns. However, because the manufacturing methods for the test splines were unknown, manufacturing processes were studied and, using precision measurement data, conclusions have been draw as to how each spline was generated.

Chapter 8 Conclusions and Recommendations

With the objective of better understanding, describing, and predicting tooth engagement in spline couplings, this research has conducted an analysis of extensive data from spline profile measurements and analytically recreated torque-deflection curves to compare with experimental results. Differences and similarities were explained, errors patterns and clusters were found and potential sources were outlined.

8.1 Thesis Summary

Tooth engagement in spline couplings is complex and difficult to predict due to variation and errors that arise from manufacturing tools and processes. Due to very small errors, spline coupling teeth do not engage simultaneously, but rather tend to engage sequentially. As a result of sequential engagement, the first tooth pair to engage will carry more load than the succeeding tooth pairs and will therefore deflect the most and fail sooner.

In order to better understand tooth engagement, this thesis has extensively studied real inspection measurement data of a spline coupling provided by an industrial partner, who also performed torque-deflection tests. The analysis of the individual splines revealed the variation associated with the roots and tips of each tooth and identified error patterns and potential causes of the variation.

After presenting the variation associated with the individual splines, this thesis presented an analytical method of simulating the tooth engagement of the assembled spline. The analytical engagement model required the actual tooth-to-tooth clearance values and the tooth stiffness values of the splines in order to re-create a torque-deflection curve for comparison with the experimental results. The clearance values were determined by locating the contact region between two mating flanks, then calculating the angular rotation required to close the gap. It was shown that the contact zone was not at the pitch circle for this particular spline coupling, but rather was located further out radially. This had a significant influence on the mating tooth stiffness and resulting tooth engagement. The clearances between each tooth pair was calculated and plotted as a function of tooth number. The spline coupling was analyzed in each of the 65 different configurations in order to find the configuration for which the overall variance was minimized and the configuration for which it was maximized.

A method of estimating tooth stiffness constants was reviewed and applied to the 65 tooth spline. An equivalent tooth pair stiffness constant was calculated. Using the tooth pair stiffness and clearance data, the tooth engagement sequence was predicted. Sample torque-deflection curves for the spline coupling were created for the two extreme variation configurations. These results were compared to results from DeCaires' models and the industrial partner tests. While the DeCaires' spreadsheet and models used statistically generated clearances and assumed contact at the pitch circle, the results were comparable to the analytical results. However, the analytical results provided valuable insight on actual tooth engagement location, error clusters, and early quasi-simultaneous tooth engagement.

Common spline manufacturing methods were studied as possible sources of error patterns. The hobbing process used in generating splines was simulated with a detailed CAD model. Special considerations that must be taken in hob selection were spelled out. Several sources of error patterns were identified.

8.2 Contribution and Accomplishments

The following list summarizes the accomplishments and contribution of this thesis in the field of tooth engagement of involute spline couplings:

Detailed analysis of spline measurements

- Created a graphical model in Excel and CAD of the spline couplings using actual inspection measurement data.
- Determined error profile associated with the roots and tips of the splines and identified likely sources of the error patterns.

Analysis of manufacturing processes

- Created a graphical model of the hobbing process to illustrate the effects of hob design on spline tooth generation.
- Explained the relationship between hob selection and spline generating that determine if a design is a prime, common, or even multiple, which contributes to periodic error patterns.

Detailed analysis of tooth engagement

- Developed new tools for analysis of tooth engagement, like profile plots, that reveal patterns and sorted tooth engagement plots to reveal error clusters.

- Calculated tooth stiffness constant values for the internal and external spline teeth.
- Calculated equivalent tooth pair stiffness value for spline coupling.
- Determined actual contact zone where tooth flanks engage, which was greater than the assumed location at the pitch circle. Resulting in modified stiffness values and tooth engagement sequences
- Created a method for determining the engagement sequences for a spline coupling for any configuration in which they may be assembled.
- Determined tooth pair clearances and engagement sequences for tooth pairs in each of the 65 different configurations.
- Identified patterns in clearance and engagement profiles and potential sources of these patterns.

Analysis of experimental results and setup

- Analyzed the experimental setup and determined likely areas where unwanted deflections were occurring.
- Provided a better understanding of the experimental torque-deflection curves and what they were measuring by comparing the analytical model with the experimental results.

The main contributions of this work are: A process for analytically creating torque-deflection curves in any configuration using measurement data, confirmation of the analytical tooth engagement sequence model from measured variation data, a better understanding of the experimental results, how to design future experimental tests, and the importance of early quasi-simultaneous tooth engagement.

8.3 Conclusions

Tooth engagement in involute spline couplings differs from coupling-to-coupling and from one configuration to the next. This has been effectively demonstrated with the industrial partners' spline coupling measurements. Initially, it may appear the spline coupling configuration with the least overall variation would be the best choice; however, it has been shown that early quasi-simultaneous tooth engagement may improve a spline coupling's load bearing capacity more than strictly reducing overall variation. In terms of overall variation, it has been shown that the largest contributor of overall variation in spline couplings comes from a periodic error pattern that is likely a result of eccentricity error in a hobbing or other generating process. When eccentricity error is eliminated, the overall variation is dramatically reduced; which emphasizes the importance of tool setup and manufacturing processes. It has also been shown that hob selection is important in spline generation and how hobbing can contribute to error patterns on external splines.

The experimental test results and design setup provided invaluable understanding of tooth engagement in spline couplings. For example, a new metric for spline performance could be used to convey the importance of early quasi-simultaneous tooth engagement in addition to overall variation. From these results, new analytical models were created to estimate tooth engagement and torque deflection curves for the spline coupling. It has also been shown how different components of the design setup may have contributed to the experimental results and what measures should be taken in order to isolate the setup to gather spline tooth engagement data.

This work has revealed many important aspects of spline coupling tooth engagement. Sequential tooth engagement has been confirmed analytically; however,

there is an additional component of clustered tooth engagement that should be taken into account. A statistical model is good in predicting tooth engagement with only random error. When strong error patterns exist, an analytical model better estimates actual tooth engagement. If an inspection program were created, using a process like that outlined in this thesis, then the optimal configuration could quickly be determined for a given spline coupling prior to assembly, thereby increasing its load carrying capacity. Marking the spline would permit re-assembly in the selected configuration. Further experiments and analysis will continue to increase understanding and aid the development of improved spline couplings.

8.4 Recommendations for Future Work

During the course of this research, many things were considered that may further spline tooth engagement theory. They are summarized below as additional areas that may be explored by future researchers.

Additional testing: With what we have learned from this study, a new experiment should be conducted. Much work and preparation could be put into a new design setup in which fixture stiffness does not obscure the results and internal slippage is eliminated. This is not an easy task and will require great care and attention to every detail in both the hardware and software. This new setup would then be able to provide clearer data to show the tooth engagement points. A new test design should not be limited to improving the current setup, but should also consider completely new tests with different technologies. For example, remove the splines and measure the stiffness of just the test setup, so it can be removed analytically. Another method is to find a setup to

measure the relative rotation immediately before and after the spline. This is similar to a standard tensile test, in which an extensometer measures change in length of a gage length on the specimen.

Automate the spline coupling engagement analysis: The steps used in analyzing the tens of thousands of data points collected from the inspection process could be automated in order to more efficiently apply this method to sets of spline measurement data. An automated process could then be used upstream by the spline manufacturer in order to improve their manufacturing processes to reduce variation.

Tool sharpening: This is an area of significant importance in spline manufacturing. Once a hob or broach is re-sharpened an entirely new set of variations is introduced to the succeeding splines manufactured. Because of this, tools may be intentionally designed to account for the material removal that occurs during a re-sharpening process.

Three-dimensional considerations: This work has limited its scope to two dimensions; however, additional work can be done in the 3rd dimension, both in hob selection consideration and in tooth engagement.

Full finite element analysis: The analytical model presented herein calculated the stiffness values and clearances for all tooth pairs, which aids in understanding tooth engagement. A full FEA might reveal other behavior to supplement tooth engagement theory, like modeling and predicting contact location between mating tooth pairs. A full FEA model will be very complex due to the fine meshing required, difficulty of including clearance variations, and the complicated boundary conditions of teeth deflecting and

more teeth engaging. Such a model would require deep understanding of FEA principles and extreme computing power.

Statistical model: Significant statistical model development remains on spline tooth engagement. For example, can error clusters, or early quasi-simultaneous tooth engagement, be modeled statistically? Can statistical models be used to help find deliberate error patterns that increase load sharing among the first tooth engagement pairs?

Optimum spline design: Conduct a sensitivity analysis of various spline parameters and their effect on tooth engagement, load share, stress, etc. Examine parameters such as: the magnitude of clearance variation, Diametral pitch, pressure angle, number of teeth, etc. Develop a design procedure and search for optimal designs for a representative set of applications. Plot tooth engagement and load share results versus spline parameters as charts for designers.

References

1. ANSI B92.1-1970, Involute Splines and Inspection, SAE, Warrendale, PA, 1993.

2. Buckingham, Earle (1935). *Manual of Gear Design Section Two,* The Industrial Press.

3. Cleghorn, William L.. Mechanics of Machines 2005 Oxford University Press, Inc. New York, Oxford

4. Colbourne, John R.. (1987). *The Geometry of Involute Gears,* Quinn Woodnine.

5. Dallas, Daniel B. (1976). *Tool and Manufacturing Engineers Handbook: A Reference Work for Manufacturing Engineers,* American Society of Tool and Manufacturing Engineers.

6. Davis Joseph R. (2005). *Gear Materials, Properties, and Manufacture,* ASM International.

7. DeCaires, Brian J.K. (2006). Variation Analysis of Involute Spline Tooth Contact.

8. Deutschman, Aaron D., et al, (1975). *Machine Design Theory and Practice,* Collier Macmillan Publishers.

9. Drago, Raymond J. (1988). *Fundamentals of gear* design, Butterworth Publishers.

10. Dudley, Darle W. (1992). *Dudley's Gear Handbook,* McGraw-Hill.

11. Dudley, Darle W. (1954). *Practical Gear Design,* McGraw-Hill.

12. Fellows Gear Shaper Company, (1964). The Art of Generating [video-recording], Springfield, Vt.

13. Jennings, Cheryl L., Kulachi, Murat, (2008). Introduction to Time Series Analysis and Forecasting, Wiley-Interscience

14. Khiralla, Tofa W.. (1976). *On the Geometry of External Involute Spur Gears,* C/I Learning.

15. Michalec, George W., Precision Gearing: Theory and Practice, John Wiler & Sons, Inc, 1966.

16. SAE Gear and Spline Technical Committee (1990). Gear Design, Manufacturing, and Inspection Manual, Society of Automotive Engineers.

17. Tennutti, Mike. Gleason Works. Hob Data Reference

Appendix A. Typical Spline Terminology [1] [7]

Diametral Pitch, P—The number of spline teeth per inch of pitch diameter.
Pitch Diameter, D—The diameter of the pitch circle, which is determined as the ratio of the number of teeth to the diametral pitch.
Pitch Point—The intersection of the spline tooth profile with the pitch circle.
Circular Pitch, p—The distance along the pitch circle between corresponding points of adjacent spline teeth.
Pressure Angle, Φ—The angle between a line tangent to an involute and radial line through the point of tangency.
Base Circle—The circle from which involute spline tooth profiles are constructed.
Base Diameter, D_b—The diameter of the base circle.
Major Circle—The circle formed by the outer-most surface of the spline. It is the outside circle (tooth tip circle) of the external spline or the root circle of the internal spline (commonly referred to the Addendum Circle in gear teeth).
Major Diameter, D_o, D_{ri}—The diameter of the major circle.
Minor Circle - The circle formed by the inner-most surface of the spline. It is the root circle of the external spline or the inside circle (tooth tip circle) of the internal spline.
Minor Diameter, D_{re}, D_i—The diameter of the minor circle.
Form Circle—The circle which defines the deepest points of involute form control of the tooth profile. This circle along with the tooth tip circle determines the limits of tooth profile requiring control. It is located near the major circle on the internal spline and near the minor circle on the external spline.
Form Diameter, D_{Fe}, D_{Fi} - The diameter of the form circle.
Depth of Engagement - The radial distance from the minor circle of the internal spline to the major circle of the external spline.
Actual Space Width, s—The circular width on the pitch circle of any single space considering an infinitely thin increment of axial spline length.
Effective Space Width, s_v—The effective space width of an internal spline is equal to the circular tooth thickness on the pitch circle of an imaginary perfect external spline which would fit the internal spline without looseness or considering engagement of the entire axial length of the spline.
Actual Tooth Thickness, t—The circular thickness on the pitch circle of any single tooth considering an infinitely thin increment of axial spline.
Effective tooth Thickness, t_v—The effective tooth thickness of an external spline is equal to the circular space width on the pitch circle of an imaginary perfect internal spline which would fit the external spline without looseness or interference, considering engagement of the entire axial length of the spline.
Effective Clearance, c_v—The effective space width of the internal spline minus the effective tooth thickness of the mating external spline.
Form Clearance, c_F—The radial depth of involute profile beyond the depth of engagement with the mating part. It allows for looseness between mating splines and eccentricities between the minor circle (internal), the major circle (external), and their respective pitch circles.

Appendix B. Methods to Make Gear Teeth [11]

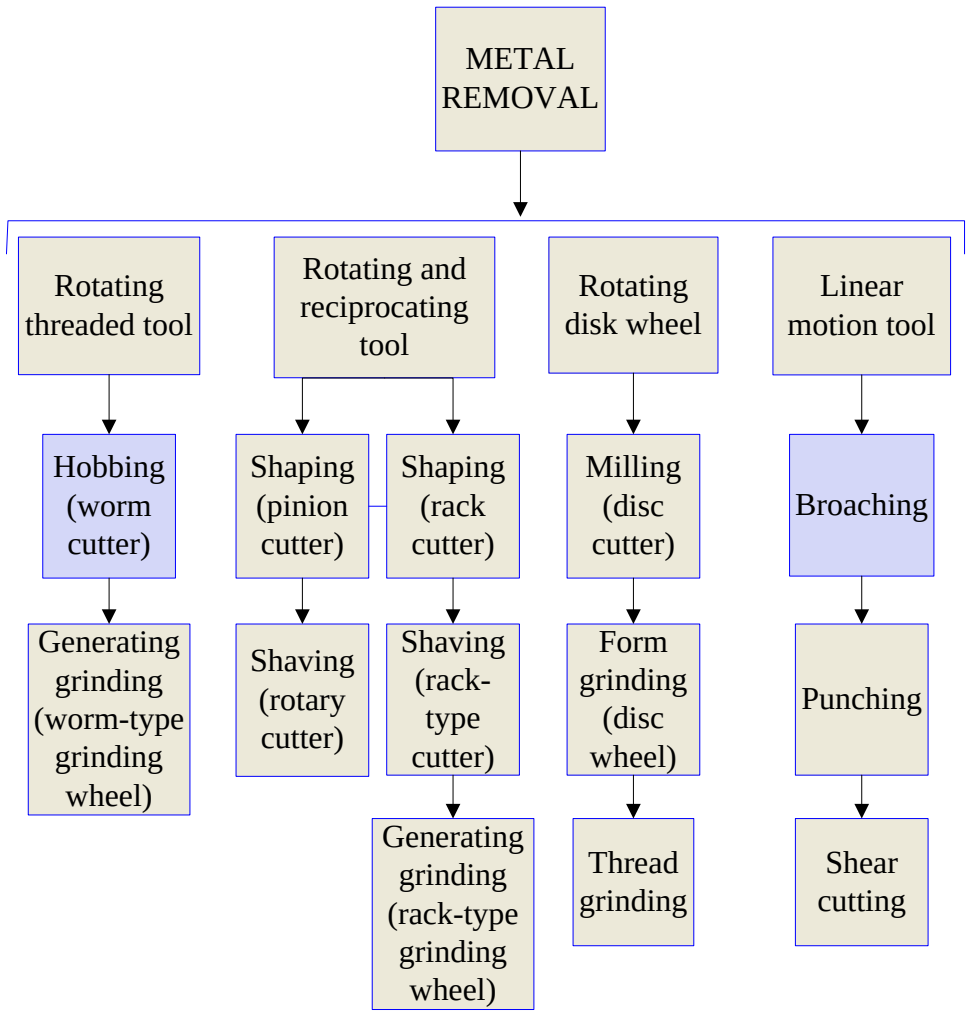

Appendix C. Sample Inspection Output

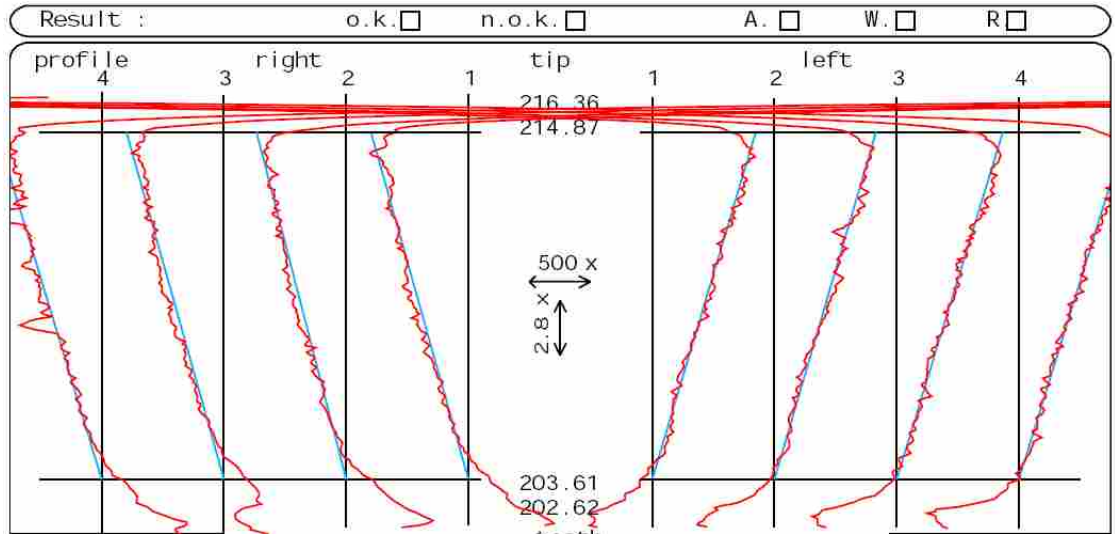

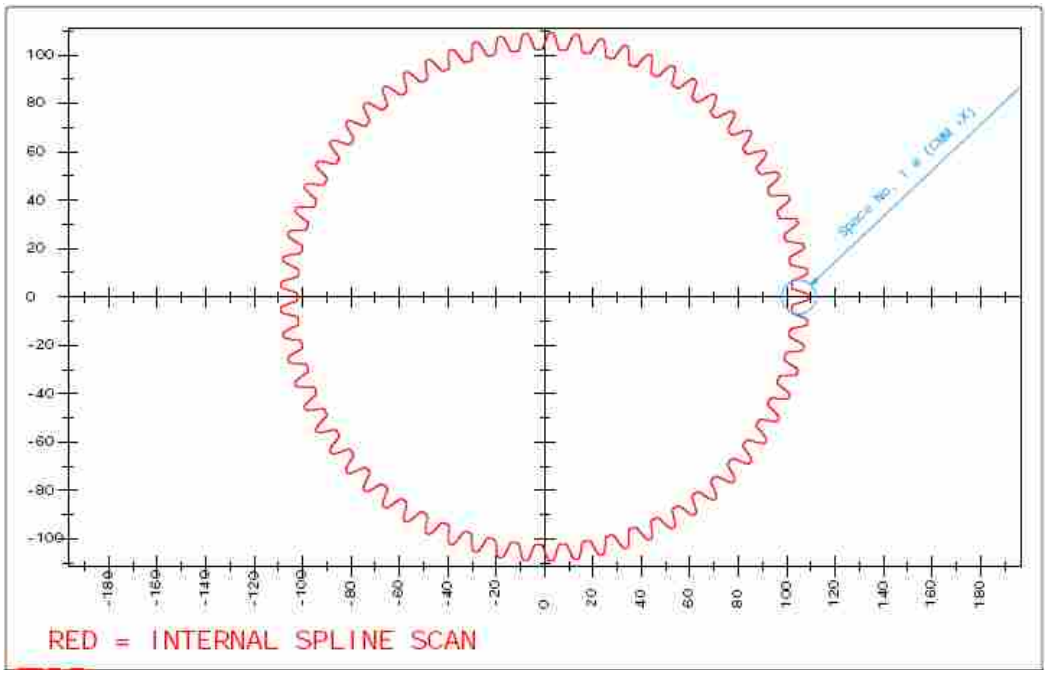

Appendix D. Stiffness Calculations

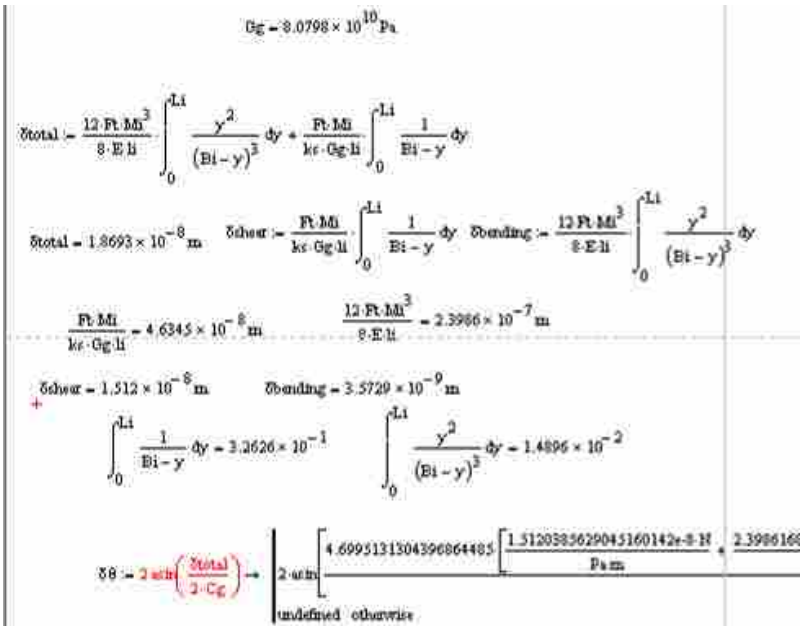

$$Gg = 8.0798 \times 10^{10}\,Pa$$

$$\delta total := \frac{12 \cdot Ft \cdot Mi^3}{8 \cdot E \cdot li} \cdot \int_0^{Li} \frac{y^2}{(Bi - y)^3}\,dy + \frac{Ft \cdot Mi}{ks \cdot Gg \cdot li} \cdot \int_0^{Li} \frac{1}{Bi - y}\,dy$$

$$\delta total = 1.8693 \times 10^{-8}\,m \qquad \delta shear := \frac{Ft \cdot Mi}{ks \cdot Gg \cdot li} \cdot \int_0^{Li} \frac{1}{Bi - y}\,dy \qquad \delta bending := \frac{12 \cdot Ft \cdot Mi^3}{8 \cdot E \cdot li} \cdot \int_0^{Li} \frac{y^2}{(Bi - y)^3}\,dy$$

$$\frac{Ft \cdot Mi}{ks \cdot Gg \cdot li} = 4.6345 \times 10^{-8}\,m \qquad \frac{12 \cdot Ft \cdot Mi^3}{8 \cdot E \cdot li} = 2.3966 \times 10^{-7}\,m$$

$$\delta shear = 1.512 \times 10^{-8}\,m \qquad \delta bending = 3.5729 \times 10^{-9}\,m$$

$$+$$

$$\int_0^{Li} \frac{1}{Bi - y}\,dy = 3.2626 \times 10^{-1} \qquad \int_0^{Li} \frac{y^2}{(Bi - y)^3}\,dy = 1.4896 \times 10^{-2}$$

$$\delta\theta := 2 \cdot \asin\left(\frac{\delta total}{2 \cdot Cg}\right) \rightarrow \begin{cases} 2 \cdot \asin\left[4.6995131304396864485 \cdot \left[\frac{1.5120385629045160142e\text{-}8 \cdot N}{Pa \cdot m} + \frac{2.3986166}{} \right. \right. \\ \text{undefined otherwise} \end{cases}$$

$$\delta shear := \frac{Ft \cdot Mi}{ks \cdot Gg \cdot li} \cdot \int_0^{Li} \frac{1}{Bi - y}\,dy \qquad \delta bending := \frac{12 \cdot Ft \cdot Mi^3}{8 \cdot E \cdot li} \cdot \int_0^{Li} \frac{y^2}{(Bi - y)^3}\,dy \qquad \delta total := \delta bending + \delta shear$$

$$\delta total := \frac{12 \cdot Ft \cdot Mi^3}{8 \cdot E \cdot li} \cdot \int_0^{Li} \frac{y^2}{(Bi - y)^3}\,dy + \frac{Ft \cdot Mi}{ks \cdot Gg \cdot li} \cdot \int_0^{Li} \frac{1}{Bi - y}\,dy$$

$$Bi := .009936 \cdot m \qquad E := 30 \cdot 10^6 \cdot psi = 2.0684 \times 10^{11}\,Pa$$

$$Li := .002766 \cdot m \qquad ks := \frac{5}{3}$$

$$rmi := .004316 \cdot m$$

$$Mi := \frac{Bi}{rmi} \rightarrow 2.3021316033364226135$$

$$li := .00318 \cdot m$$

$$Cg := .106394 \cdot m \qquad \nu := .28$$

$$\theta id := 23.48$$

$$Gg := \frac{E}{2 \cdot (1 + \nu)}$$

$$\theta r := \theta id \cdot \frac{\pi}{180}$$

$$\theta r = 4.098 \times 10^{-1} \qquad Tg := 1 \cdot N \cdot m$$

$$Ftotal := \frac{Tg}{Cg} \rightarrow 9.399026260879372897 \cdot N$$

Appendix E. Hob Nomenclature (ANSI/AMGA 1102-A03)

Adjacent flute spacing: the variation from the desired angle between adjacent tooth faces measure in the plane of rotation.

Adjacent thread spacing: the difference in the average variations obtained by traversing along the desired helical path of one thread, indexing and traversing in a similar manner on an adjacent thread.

Approach distance: the linear distance in a direction of feed between the point of initial hob contact and the point of full hob contact.

Arbor collar: a hollow cylinder which fits an arbor, and is used to position the hob.

Auxiliary leads: a feature employed on some hobs, especially worm gear hobs, wherein both sides of the hob thread have leads different from the nominal hob lead; one side longer, the other side shorter. This results in the tooth thickness being successively less toward the roughing end of the hob.

Axial feed: the rate of change of hob position parallel to the work piece axis usually specified in inches per revolution of the work piece.

Axial plane: a plane containing the axis of rotation.

Cam: the radial drop of the form in the angular distance between adjacent tooth faces.
Centering device—a ground locating pin used to center a tooth or space of the hob on the centerline of the work piece.

Climb hobbing: rotation of a hob in the opposite direction to the feed of the hob relative to the workpiece at the point of contact.

Common factor ratio: in multiple thread hobs, the condition wherein the gear tooth-hob thread ratio is not a whole number, but there is a common factor of the number of gear teeth and the number of hob threads.

Conventional hobbing: rotation of a hob in the same direction as the feed of the hob relative to the workpiece at the point of contact.

Cutting face width: the axial length of the relieved portion of the hob.
Cutting speed—the peripheral lineal speed resulting from rotation, usually expressed as surface feet per minute (sfm).

Even ratio: in multiple thread hobs, the condition wherein the gear tooth-hob thread ratio is a whole number.

Flute: a longitudinal groove either straight or helical that forms the tooth face of one row of hob teeth and the backs of the preceding row. It also provides chip space.
Flute helix angle—the angle which helical tooth face makes with an axial plane, measures on the hob pitch cylinder.

Flute lead: the axial advance of helical tooth face in one turn around the axis of a hob.
Flute lead variation—the deviation of a hob tooth face from the desired helical surface.

Full top radius: continuous radius tangent to top and side cutting edges.

Gear tooth-hob thread ratio: the ratio of the number of teeth on the workpiece to the number of threads in the hob.

Generated fillet: at the bottom of the hobbed form a fillet joining the root diameter with the desired generated form. This fillet is not a true radius.

Hob addendum: radial distance between the top of the hob tooth and the pitch cylinder. Do not confuse with gear addendum.

Hob dedendum: in topping hobs, the radial distance between the bottom of the hob tooth profile and the pitch cylinder. Do not confuse with gear dedendum.

Hob runout: the runout of hob when mounted in hobbing machine, measured radially on hub diameter, and axially on hub face.

Hob shift: the axial movement of a hob along its axis to engage a different section with the workpiece.

Hub: a qualifying surface at each end of an arbor type hob which is provided for checking diameter and face runout.

Hub diameter runout: the total variation in radial distance of the hub periphery from the axis.

Hub face runout: the total axis variation of the hub face from a true plane of rotation.

Infeed: the radial rate of change of hob position, relative to the workpiece axis, usually specified in inches per revolution of workpiece.

Lead: the axial advance of a thread for one complete turn, or convolution.

Lead angle: the angle between any helix and plane of rotation, in a hob, lead angle usually refers specifically to the angle of thread helix measured in the pitch cylinder.
Lead variation—the axial deviation of the hob teeth from the correct thread lead.

Normal Plane: A plane perpendicular to a pitch cylinder helix.

Number of Threads: In multiple thread hobs, the number or parallel helical paths along which hob teeth are arranged, sometimes referred to as number of starts. Should not be confused with the term, number of threads per inch, which is commonly used in designation of the axial pitch of screw threads.

Outside Diameter Runout: The total variation on the radial distance from the axis to the tops of the hob teeth.

Tangential Feed: The rate of change of hob position along its own axis, usually specified in inches per revolution of the workpiece.

Thread: A helical ridge, generally of constant form or profile. In a hob, unlike a worm or screw, the thread is not continuous and exists only at the cutting edges of the hob teeth. Therefore, it is sometimes referred to as the thread envelope.

Tip relief modification: a modification on the sides of the hob tooth near the bottom which produces a small amount of tip relief. Such modification is usually incorporated in finishing hobs except in the finer pitches.

Axial Tooth thickness: The tooth thickness as measured in an axial plane. \

Normal Tooth Thickness: the tooth thickness as measured along a helix normal to the thread helix.

Total Indicator Variation (tiv): the difference between maximum and minimum indicator readings during a checking cycle.

Undercut: the condition at the base of a hobbed workpiece form wherein additional material beyond the basic form is removed. Under certain conditions this may occur naturally, while in other cases it may be produced by intentional modification of the bob tooth.

Wear land: a cylindrical or flat lad worn on the relieved portion of the hob tooth behind the cutting edge.

Wobble: the motion a hob when the radial runout varies along the hob length